UNITED STATES DEPARTMENT OF THE INTERIOR

GEOLOGICAL SURVEY

Investigation of a Natural Slope Failure in Weathered Tertiary Deposits, Western Powder River Basin, Wyoming

By Alan F. Chleborad

Open-File Report 80-673

1980

CONTENTS

ILLUSTRATIONS

Tables

Investigation of a Natural Slope Failure in Weathered Tertiary Deposits, Western Powder River Basin, Wyoming

By Alan F. Chleborad

ABSTRACT

A shallow landslide in weathered Tertiary deposits south of Sheridan, Wyo., exhibited seasonal creep during and shortly after spring thaw and snowmelt in late March and early April of 1977 and 1978. Inclinometer measurements in five drill holes revealed displacement profiles comprised of three elements that define differing zones of behavior within the slide mass.

Silty clay was found to be the main material type in the slide; however, thin zones of carbonaceous clay with concentrations of selenite (gypsum) crystals were identified at points of maximum displacement in three of four inclinometer holes sampled.

Although high pore pressure was detected at one location near the head of the slide, an infinite slope stability analysis using strength parameters determined in consolidated drained direct shear tests indicate high pore pressure was not a necessary precondition for failure.

Following an unusually heavy rain in mid-May of 1978, renewed movement enlarged the slide area and deformed inclinometer casing to the extent that complete measurements could no longer be made.

INTRODUCTION

The problem of slope instability in slide-prone areas of the western Powder River Basin is a recent concern because of accelerated urban and industrial growth related to increased coal development.

Natural-slope failures are common in areas underlain by the fine-grained facies of the Tertiary Wasatch and Fort Union Formations that extend over much of the region. Lithologies of the two formations are similar, and consist mostly of continental deposits of claystone, siltstone, sandstone, shale, and coal (Taff, 1909; Mapel, 1959). The beds dip gently to the east away from the Bighorn Mountain front and vary considerably in thickness and lateral extent. Eocene time-depositional environments included alluvial-fan and braided-stream systems, which flanked the Big Horn uplift, to broad alluvial plains with swamps, lakes, and levee and crevasse-splay systems farther east (Obernyer, 1978). Erosion of several thousand feet of Tertiary sediment during the late Cenozoic exhumed the Bighorn Mountains (McKenna and Love, 1972), leaving, at its eastern flank, an irregular topography locally dominated by dissected flat pediment surfaces, rounded hills, and north-trending elongate ridges.

In the vicinity of Sheridan, Wyo., various types of landslide movement occur, including translational, flow, and rotational movements in the form of debris and slab slides, earthflows, slumps, and occasional small mudflows. Commonly, the slides are complex and display more than one type of movement.

One of these slides, on a ranch 12 km south of Sheridan, Wyo., was chosen for detailed study in the fall of 1976 (fig. 1). The slide, which is at the head of a small east-trending drainage, is underlain by beds of the Wasatch Formation that dip approximately 1° to the east. The slide was chosen because of easy access and because it is representative of many of the slides in total area (750 m^2), slope angle (11°), associated slope aspect (N. 66° E.), and estimated thickness (3 m) (Chleborad and others, 1976). Additionally, the slide was a recent occurrence (spring of 1973) and had surface indications of fresh movement in the spring of 1976. In August of 1976, the landslide was drilled, sampled, and instrumented to investigate material properties and water conditions, and to determine the location and nature of the failure zone.

ACKNOWLEDGMENTS

The author gratefully acknowledges the support and technical assistance of J. B. Bennetti, T. F. Bullard, D. S. Collins, W. F. Ebaugh, G. S. Erickson, H. D. Gomez, A. T. Jenkins, H. Y. Ko, C. H. Miller, T. C. Nichols, J. K. Odums, H. W. Olsen, F. W. Osterwald, P. S. Powers, W. K. Smith, and W. Z. Savage, all of the U.S. Geological Survey.

Mr. and Mrs. C. A. "Dick" Springer permitted access to their property and provided useful information. Their generosity and cooperation is greatly appreciated.

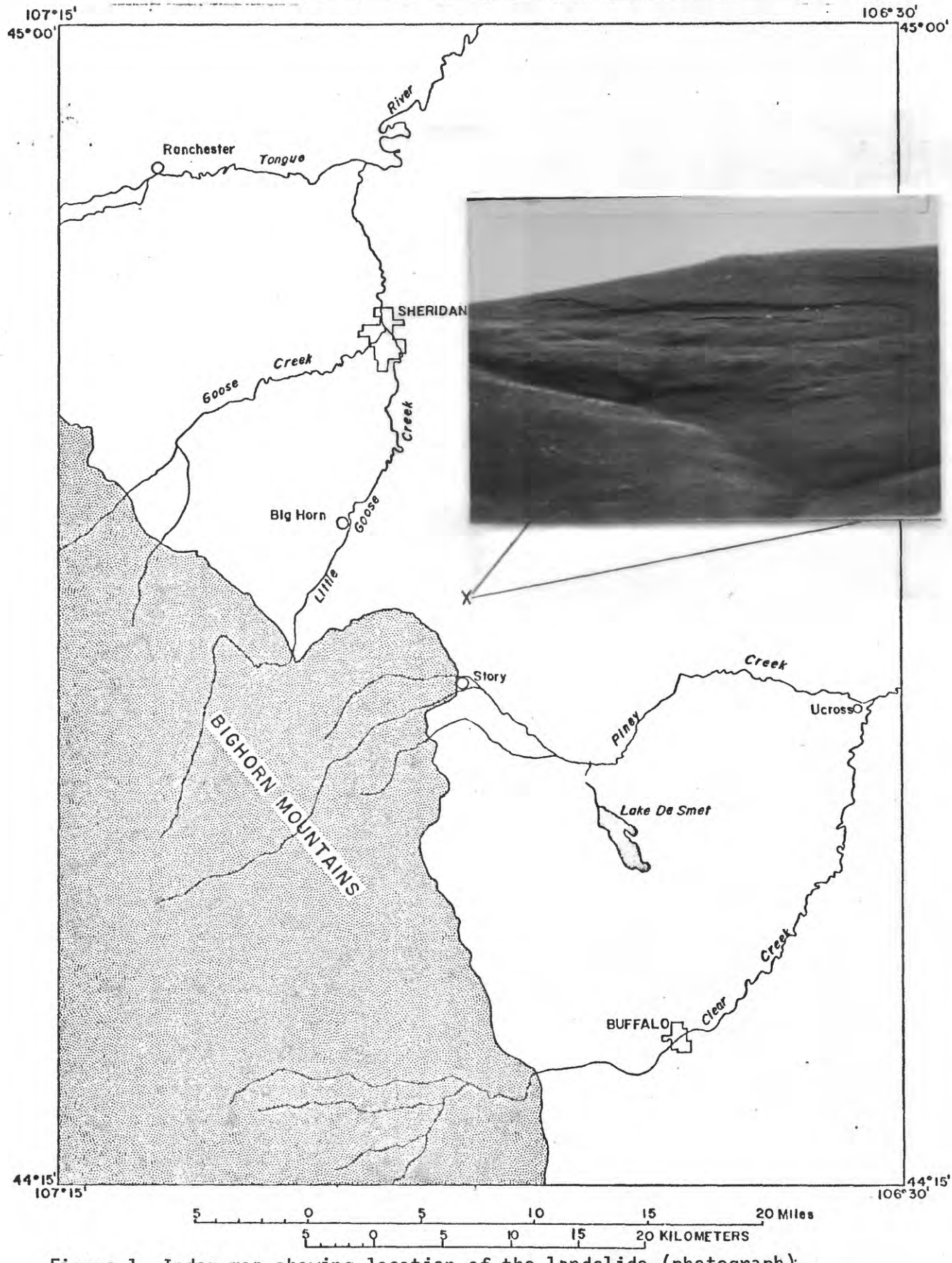

Figure 1. Index map showing location of the landslide (photograph) approximately 8 mi (12 km) southeast of Sheridan, Wyo. Note sheep at head of slide for scale.

PREVIOUS WORK

Ebaugh (1977) presented geotechnical properties logs from four boreholes (three on the slide and one off), relating lithology with pocket-penetrometer values, Atterberg limits, moisture contents, densities, and grain-size distributions. Lithologies found in the boreholes were described as predominantly sandy to silty clay with thin, interbedded, fine to coarse sand and carbonaceous clay. A poorly defined, 1-2 m thick, colluvial layer of sandy silt and silty to sandy clay mantles the slope. Reported pocket-penetrometer strength indices are generally less than 4.0 kg/cm^2 in near-surface weathered material, and generally higher than 4.0 kg/cm^2 in deeper and relatively unweathered material. A Morgenstern-Price slope stability analysis and an infinite slope analysis were made using strength properties obtained from triaxially tested core samples of silty clay taken from the slide mass. The testing yielded an effective angle of internal friction value of 26.8° and an effective cohesion of 11.0 kPa. For the purpose of the analysis those strength properties were assumed to be uniform throughout the slope. The Morgenstern-Price analysis indicated that high artesian pore water pressure was necessary to induce failure. Results of the infinite slope analysis, for a saturated condition lacking artesian pore-water pressure, indicated stability for slopes less than 25°. It was noted that the Wyoming Highway Department (WHD) measured significantly lower strength values for clayey samples taken from similar slopes during the construction of Interstate Highway 90, 1 km to the east. Plots based on the infinite slope analysis of depth to failure versus slope angle, using the WHD strength values and those measured for the landslide, indicate widely varying angles of instability.

A geophysical investigation to determine seismic properties of the landslide was conducted by Miller and others (1979) in the spring of 1977. On the basis of compressional-wave velocities they concluded that a low-velocity layer varying between 4.5 and 8 m in thickness overlies a high-velocity layer. A velocity contrast was not detected between the landslide and adjacent undisturbed ground. Shear modulus and other elastic moduli, based on velocity and density measurements for the low-velocity layer, was found to be about one-tenth that of the high-velocity layer. It was concluded that the low-velocity layer defines a relatively low-strength mantle of colluvium and unconsolidated and weathered bedrock, and the high-velocity layer defines relatively high-strength bedrock.

PRESENT STUDY

This study was undertaken to determine the location and conditions of failure within the slope and to identify geologic factors that influence slope stability. The findings are based on inclinometer and piezometer data collected at the site during a 1-1/2-year period between August 1976 and May 1978. Information on the depth of slide movement provided by the inclinometer data led to a closer examination of core sample from zones of movement. A stereo-zoom (15-37.5X) laboratory microscope was used for the preliminary identification of mineral associations and to examine micro-structure. X-ray and chemical analyses were performed on selected samples to determine composition and variations in mineralogy. Particle-size analyses, Atterberg limit determinations, consolidation tests, and consolidated drained direct-shear tests were also performed on selected samples.

DRILLING AND SAMPLING

Drilling was accomplished with a Mobil B-52[1] auger core drill. A total of five inclinometer holes and three piezometer holes were drilled at the locations and to the depths indicated in figure 2. The drill holes were designated as follows: CHP/CHW (piezometer holes near the center of the head of the slide), CHI (center head inclinometer hole), NFI and SFI (north- and south-flank inclinometer holes), CMI (center middle inclinometer hole), CFI (center foot inclinometer hole), CMP (center middle piezometer holes) and NOW (piezometer hole north of the landslide). Continuous Shelby[1] tube core samples (7 cm diameter) were taken from boreholes CHP/CHW, CMI, NFI, CFI, and NOW. Due to increased resistance to drilling, sample from 7.4 to 14.7 m in borehole CHW was obtained using NX-wireline core barrels. Some of the core was hydraulically extruded from Shelby tubes and examined at the site; the remaining tubes were sealed and shipped to the laboratory for examination and testing. Sample depths were obtained by measuring piston throw to the nearest one-half inch (1.29 cm) before and after push of a Shelby tube and by measuring hole depth after sample extraction. As an additional check on recorded depths, sample lengths were measured after extrusion from the Shelby tubes.

[1]The use of trade names is for descriptive purposes only and does not necessarily constitute endorsement by the U.S. Geological Survey.

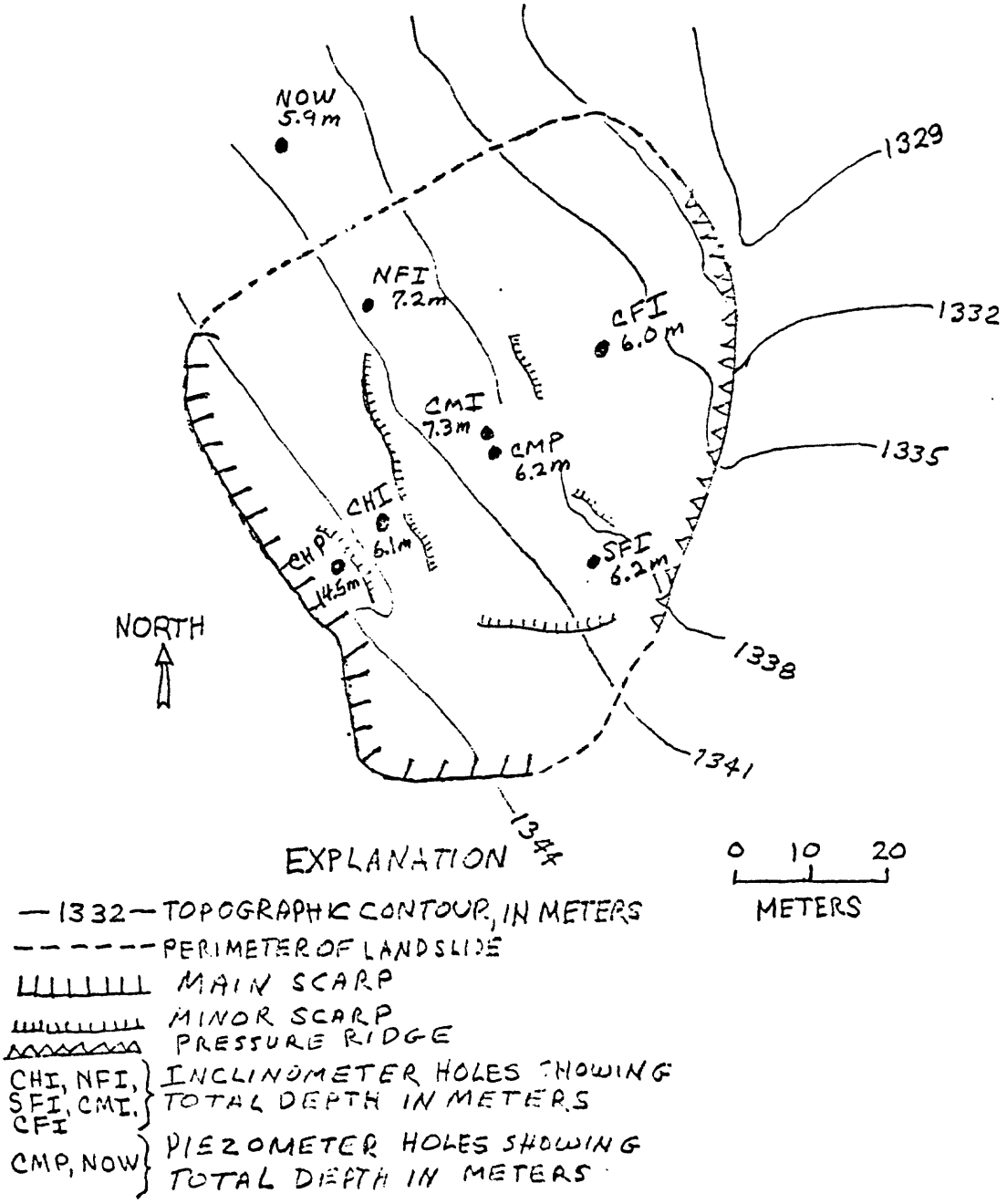

FIGURE 2: LANDSLIDE MAP SHOWING MORPHOLOGIC FEATURES AND DRILLHOLE LOCATIONS.

INCLINOMETER MEASUREMENTS

Installations and Instrumentation

Aluminum inclinometer casing (5.9-cm ID, 0.16-cm wall thickness) was installed in drill holes CHI, CMI, NFI, SFI, and CFI using an annular sand-packing technique described by Ebaugh and others (1977). Casing segments, 3.05 m in length, were joined with aluminum couplings and lowered into the boreholes. Sand was poured around the casing and saturated to a fluid condition to settle and compact, thus eliminating air pockets between the casing and the borehole wall. A biaxial miniprobe digital inclinometer was used to detect slide movement. Details of the probe, its calibration, and use are given in the appendix.

Data Collection

Initial readings were taken in the fall of 1976 immediately after installation of the inclinometer casing. Subsequent readings were made in the spring and early summer of 1977 and in the spring of 1978.

1977 Measurements

One set of readings was obtained from inclinometer hole CMI in the middle of the slide, prior to spring thaw, on April 2, 1977. The readings were made after digging through a 1- to 2-m-deep snowdrift that covered the slide. Conditions prevented measurement in the other holes. Readings were taken in all the holes on April 15, by which time all the snow had melted. Subsequently, complete readings were taken on May 19 and June 23, 1977.

1978 Measurements

Circumstances similar to those in 1977 prevailed prior to spring thaw in 1978. Inclinometer-hole CMI was monitored March 13, after digging through nearly 1.5 m of drifted snow. By March 24, 0.7 m of snow had melted, and readings were taken in inclinometer-holes CMI, SFI, NFI, and CFI. Deep snow prevented the monitoring of CHI at the head of the slide. Readings were then taken on April 4, after total snowmelt, in all the inclinometer holes. In mid-May 1978, an unusually heavy rainstorm occurred, leaving 96 mm of rain and raising the month's total precipitation to 153 mm--exceeding a 40-year mean for the month by 90 mm. An inspection of the slide after the rainstorm revealed new fractures and enlargement of the slide area. The movement deformed inclinometer casings in all the boreholes to the extent that complete measurements could no longer be made, and thus 1 1/2 years of data gathering ended.

Displacement Profiles

Displacement-depth graphs showing horizontal displacement of the boreholes relative to initial positions (vertical axes) are shown in figures 3-7. Resultant displacements were obtained by vectorially summing readings from orthagonal axes of measurement. The profiles are cumulative from the bottom up. It can be seen that the bottom of the casing in each borehole shows no significant movement and thus can be considered a fixed datum relative to that above. Anamolous negative displacements recorded on April 2, 1977, in borehole CMI (fig. 5) are assumed to result from casing settlement after installation.

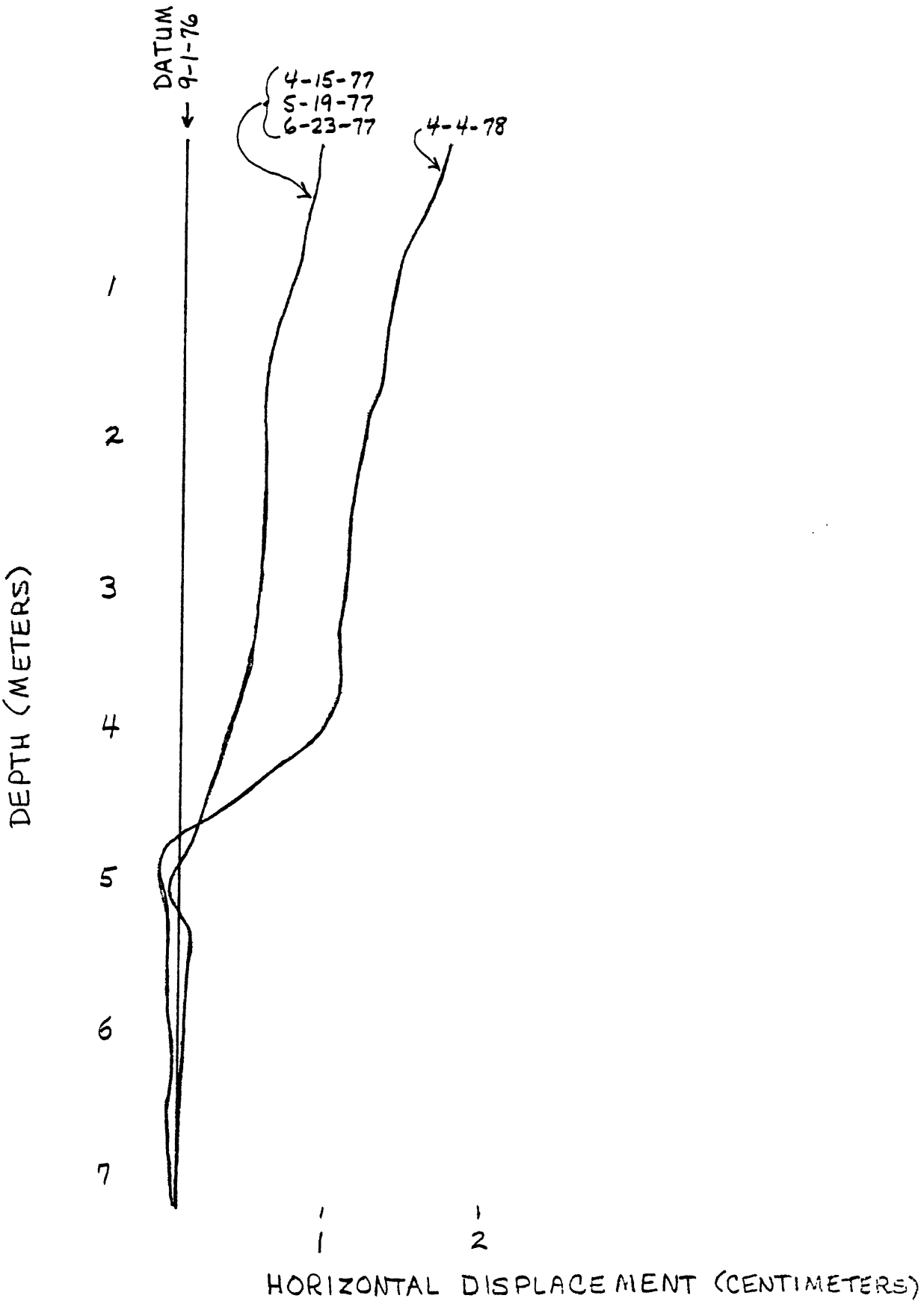

FIGURE 3 : CUMULATIVE DISPLACEMENT-DEPTH PROFILES FOR THE CENTER HEAD INCLINOMETER HOLE (CHI).

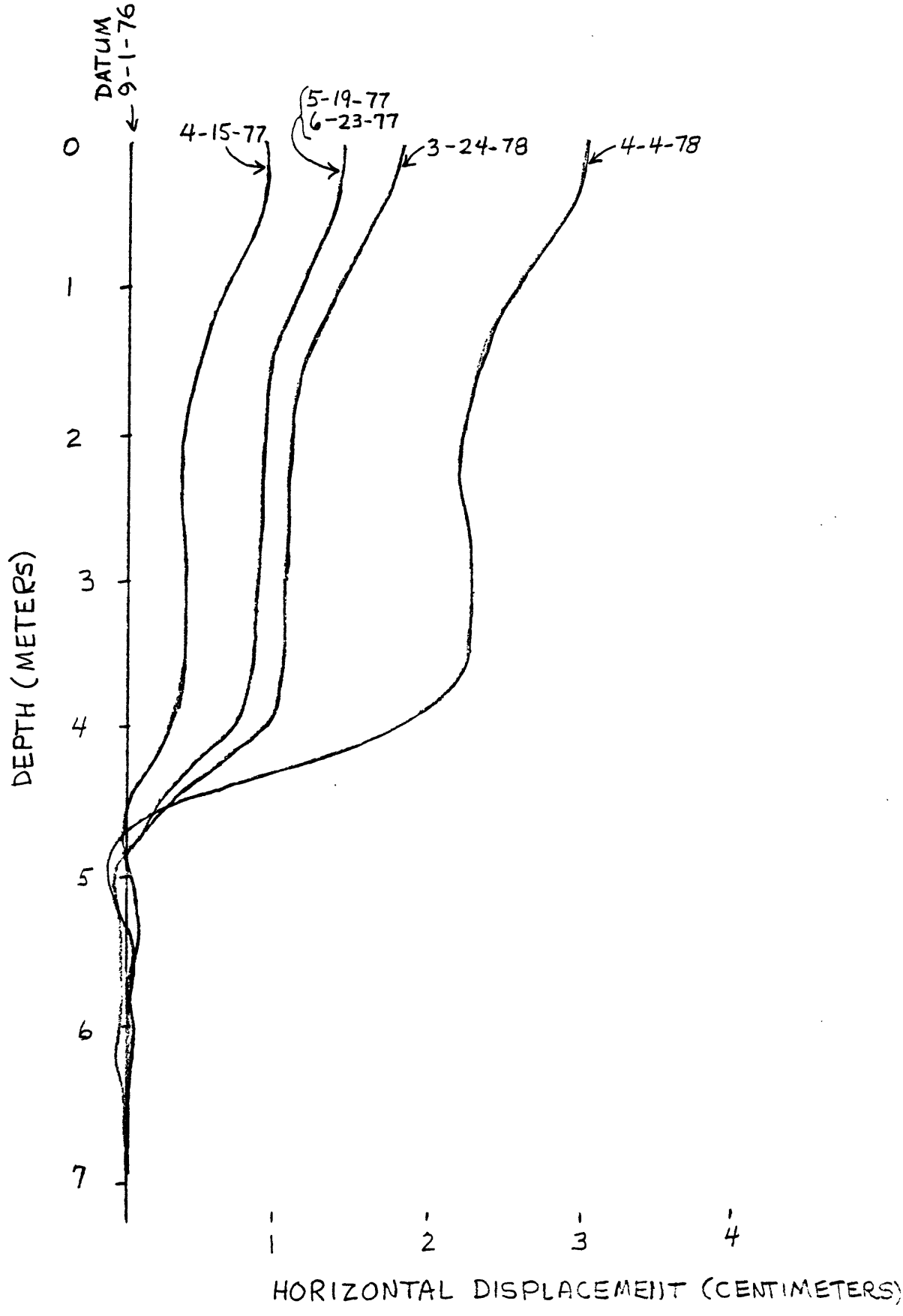

FIGURE 4: CUMULATIVE DISPLACEMENT - DEPTH PROFILES FOR THE NORTH FLANK INCLINOMETER HOLE (NFI).

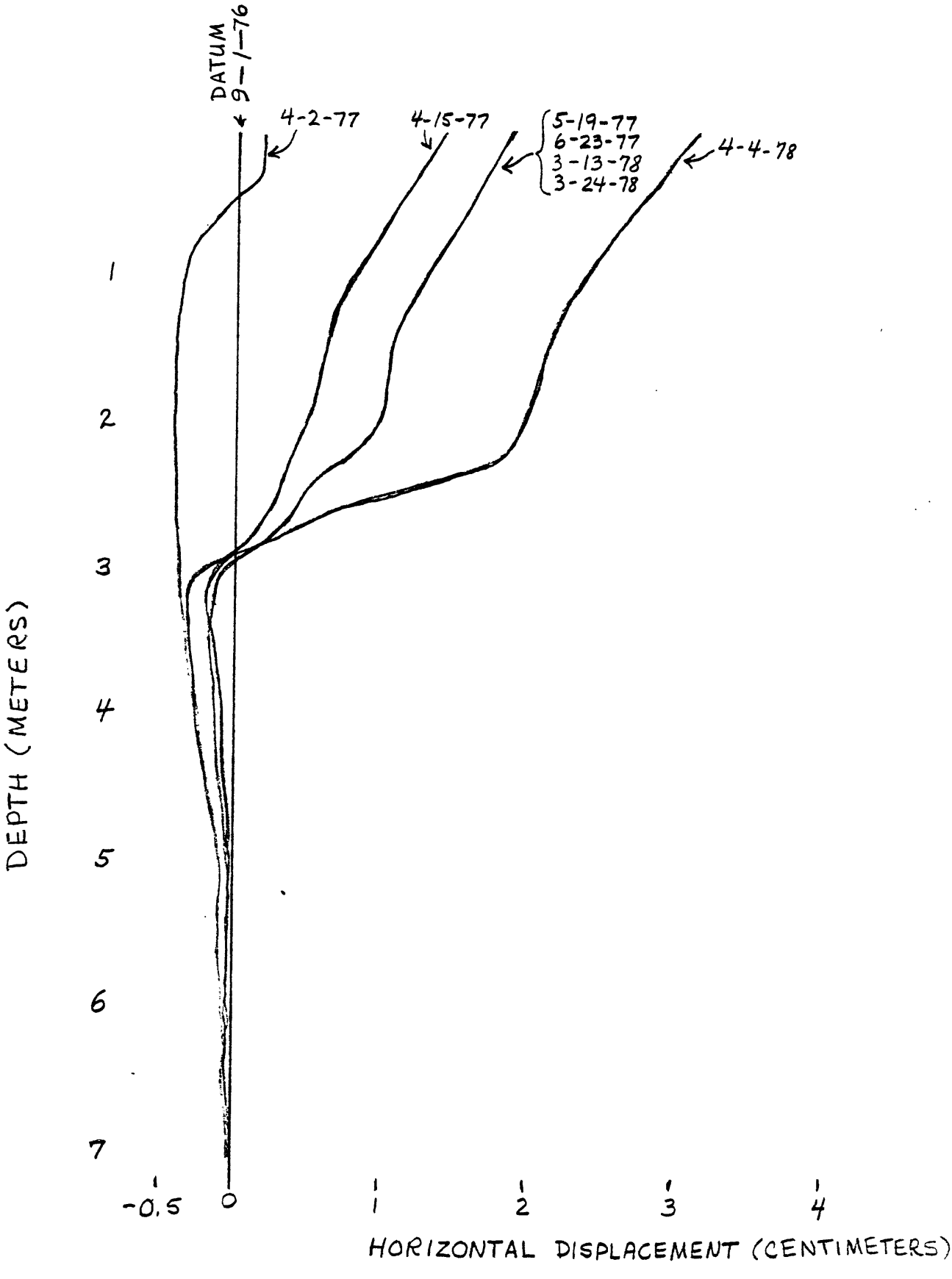

FIGURE 5: CUMULATIVE DISPLACEMENT- DEPTH PROFILES FOR THE CENTER MIDDLE INCLINOMETER HOLE (CMI).

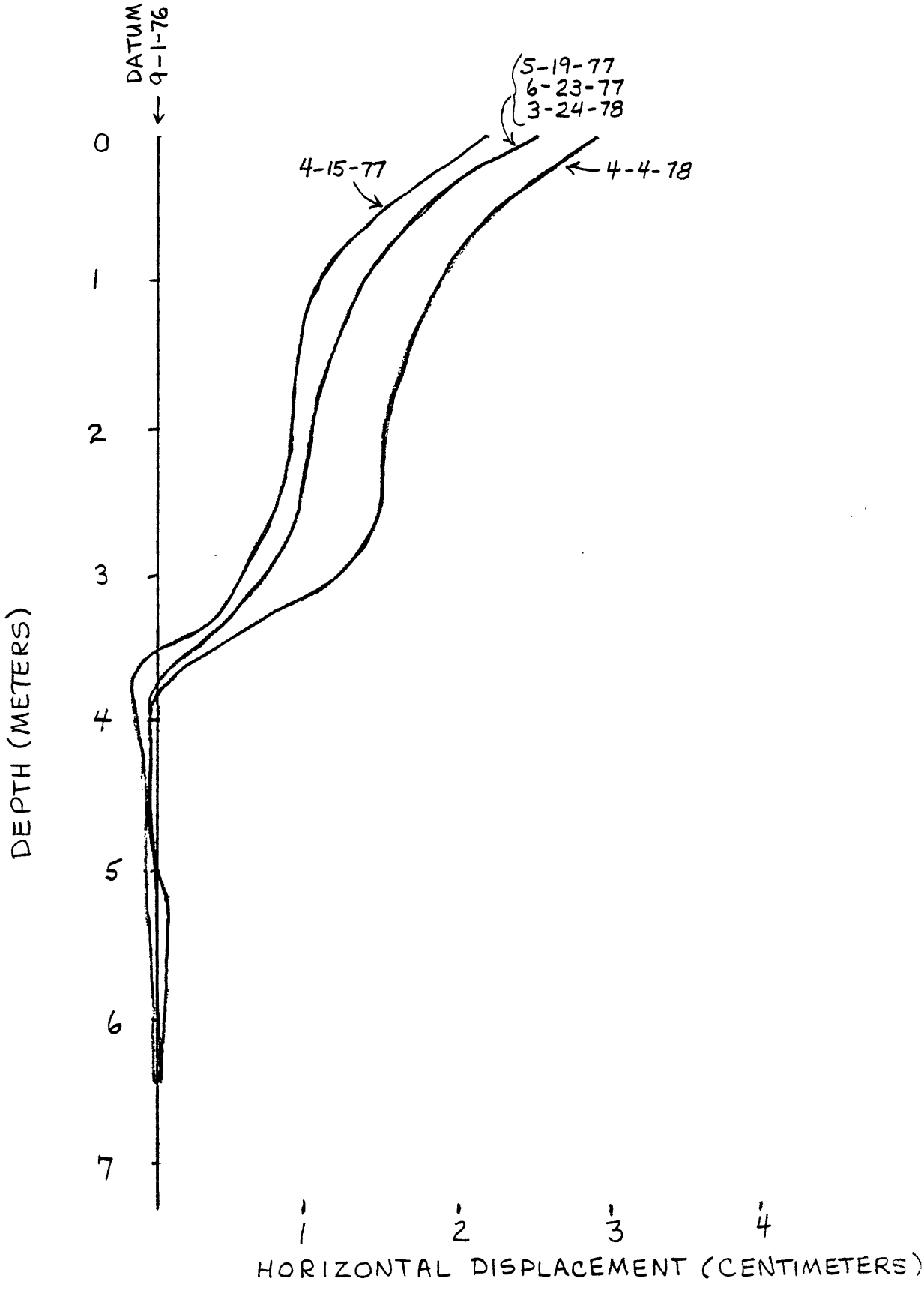

FIGURE 6: CUMULATIVE DISPLACEMENT-DEPTH PROFILES FOR THE SOUTH FLANK INCLINOMETER HOLE (SFI).

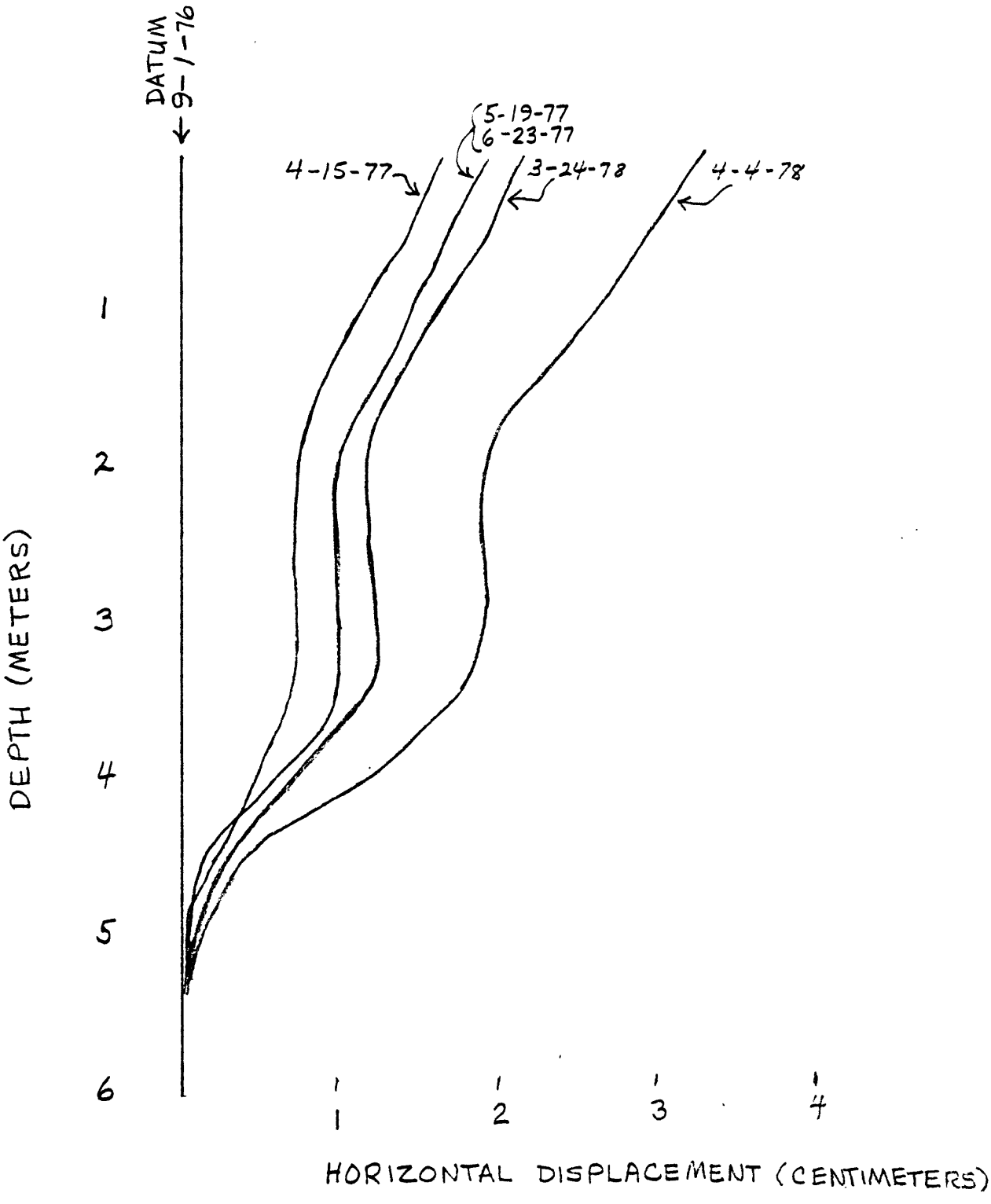

FIGURE 7: CUMULATIVE DISPLACEMENT-DEPTH PROFILES FOR THE CENTER FOOT INCLINOMETER HOLE (CFI).

The first significant movement is indicated by the profile dated April 15, 1977. The majority of movement in 1977 occurred between April 2 and 15, as indicated by the center middle inclinometer-hole profiles for those dates (fig. 5). Total movement during 1977 varied from 0.8 cm at the head of the slide (CHI) to approximately 2.0 cm at the foot (CFI) and middle (CMI) of the slide.

Similarly, in 1978, during the period March 24 to April 4, and prior to the heavy rains in mid-May, movement was renewed. Totals varied from 0.5 cm on the south flank (SFI) to approximately 1.5 cm on the north flank (NFI) during that time.

Small displacements (<0.5 cm) are indicated by the profiles for inclinometer-holes NFI, SFI, and CFI (figs. 4, 6, and 7) and occurred during the 10-month period from May 19, 1977, to March 24, 1978. Figure 8 shows the magnitude and direction of the net horizontal displacements at the top of the inclinometer holes as indicated by inclinometer data for the period September 1976 to April 1978. The movements are generally consistent in direction (north-northeast) and magnitude (2-3 cm). It should be noted that the directions of movement vary considerably from the general downslope direction indicated by the contours. This variation may be explained, in part, by the topographic high which bounds the slide on the east side, restricting movement in the downslope direction.

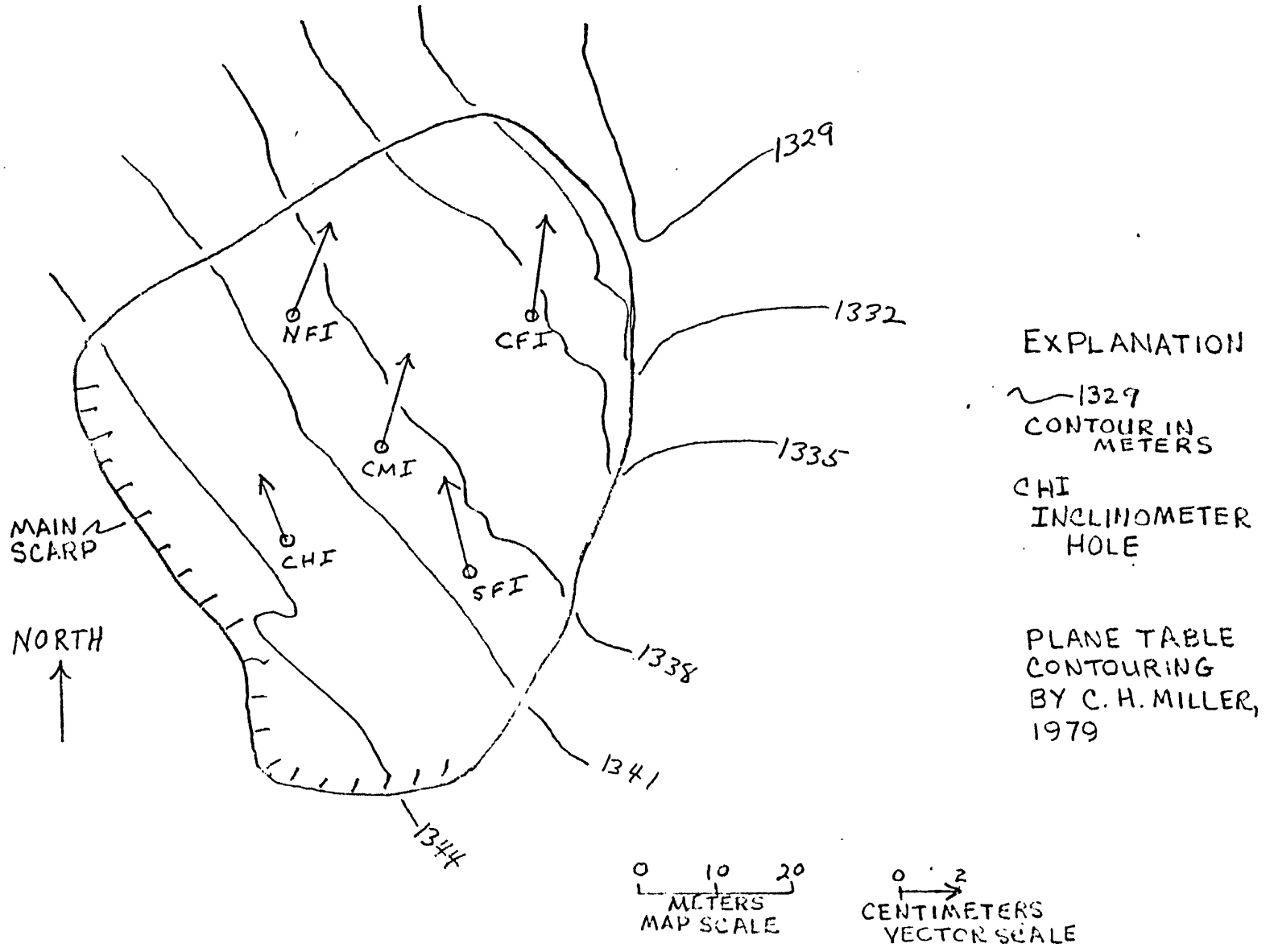

FIGURE 8: MOVEMENT VECTORS SHOWING THE MAGNITUDE AND DIRECTION OF NET HORIZONTAL DISPLACEMENT AT THE TOP OF THE BOREHOLES FOR SEVENTEEN MONTHS TO APRIL 1980 AS INDICATED BY THE

The displacement profiles from each borehole are comprised of three elements that define differing zones of behavior within the slide mass: an upper curvilinear element, interpreted as a zone of surface-creep; a near-vertical rigid element of little or no displacement; and a lower curvilinear element defining a lower creep zone. For example, the profile dated April 4, 1978, for borehole CHI (fig. 3) shows a surface creep zone between 0 and 2 m depth, a middle rigid zone between 2 and 3.7 m, and a lower zone of creep between 3.7 and 4.8 m. Renewed sliding after the heavy rains of mid-May 1978 deformed the casing in each hole at depths corresponding to the lower zone of movement. The relationship between the zones of movement, lithologies, material properties, and weathering characteristics are discussed in the later sections of this report.

PIEZOMETER MEASUREMENTS

Three hydraulically flushable electric piezometers were installed in borehole CHP at the head of the slide (fig. 2), one at 3.6 m in a medium to coarse sand, one at 4.7 m in silty clay, and the third at 5.7 m in a carbonaceous clay zone. Two electric piezometers were also installed in borehole CMP at the middle of the slide. One at 5.6 m in a sandy to silty clay and the other at 7.2 m in a fine to medium sand with a thin carbonaceous clay interbed. Well-point piezometers were installed in the same horizons near the electric piezometers as a rough check on piezometric levels. Three well-point piezometers were also installed north of the slide in borehole NOW at depths of 2.4, 3.2, and 6.1 m. Details of the piezometer installations are presented in the appendix. The inclinometer holes were used as observation wells and were the only source of water-level information at the foot and near the flanks of the slide.

Piezometer data were collected on the same dates and under the same conditions as were the inclinometer data. Data plots are presented in figures 9-11. The following ground-water conditions are evident: high pore pressure existed at 5.3 m in piezometer-hole CHP at the head of the slide during periods of spring thaw in 1977 and 1978, and after the heavy rains in May of 1978 when an artesian condition of 9 m above ground level (142 kPa pore pressure) was detected. According to Ebaugh (1977), the high pore pressure can be explained by assuming a waterhead due to bedrock dip in an aquifer 366 m long (maximum updip length at the slide locality). In 1977, the piezometric head had dropped only slightly by June 23, although creep deformation apparently ended by May 19 of that year. The piezometric levels at 4.6 and 5.3 m depth at the head of the slide did not rise above ground level. In comparison, the piezometric heads in the middle of the slide are low--never exceeding 2 m. Water levels in the inclinometer boreholes (fig. 10) also reflect the effects of spring thaw and infiltration of snowmelt, as evidenced by the rise in water level between April 1 and 15, 1977, in CMI and between March 13 and 24, 1978, in all of the inclinometer holes. The higher water levels in May of 1978 are attributed to the heavy rainfall in mid-May. Water levels were highest in the inclinometer hole at the foot of the slide (CFI) and generally lowest in the inclinometer holes at the middle (CMI) and south flank (SFI) locations. The offslide well-point piezometers (fig. 11) also show a rise in piezometric head after spring thaw in 1977 and 1978, with a high at the 6.1-m-depth measuring point of 5.7 m.

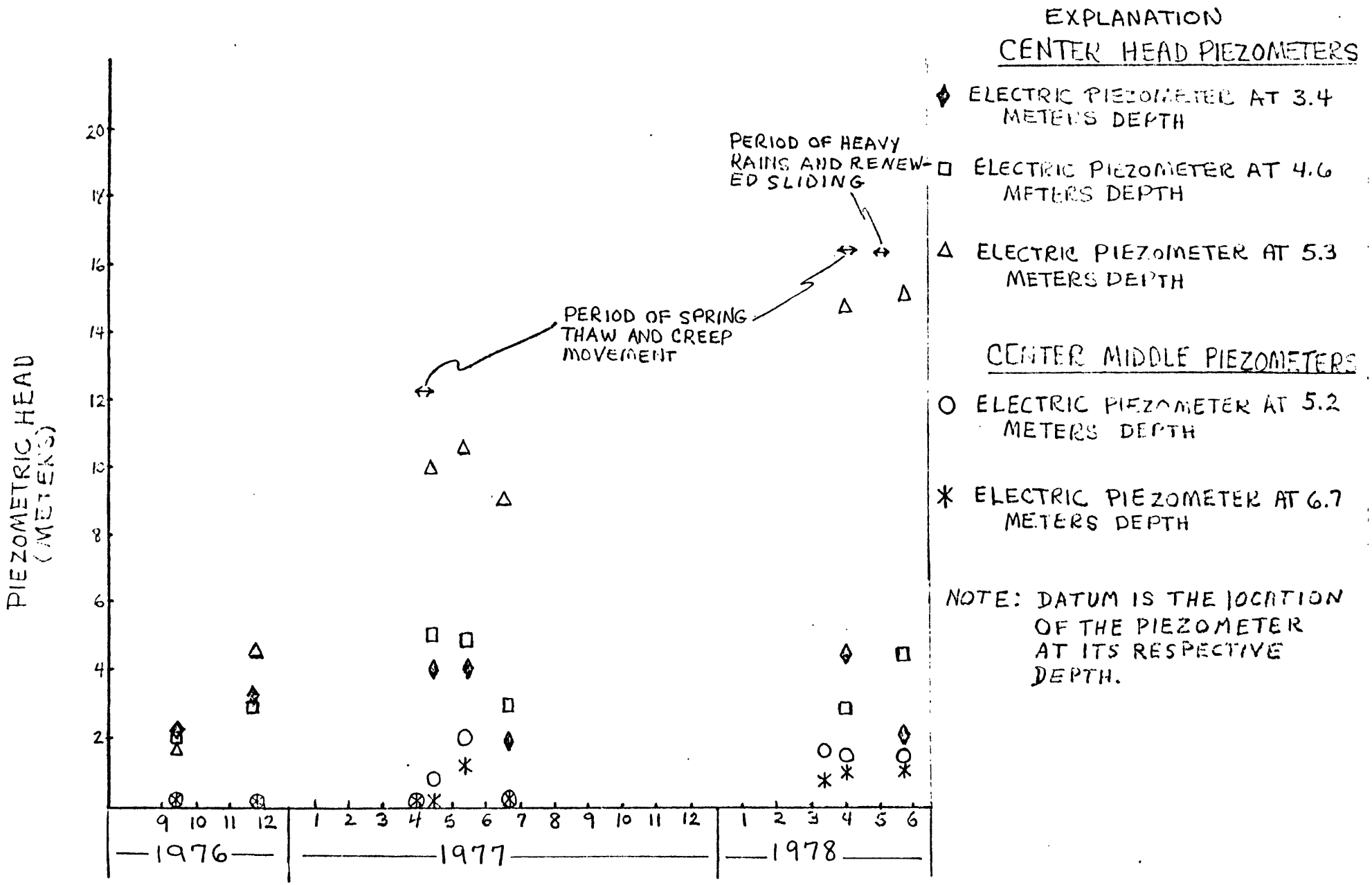

FIGURE 9 : ELECTRIC PIEZOMETER DATA SHOWING PIEZOMETRIC HEADS AT THREE MEASURING POINTS AT THE HEAD OF THE SLIDE AND TWO AT THE MIDDLE FOR SEPTEMBER 1976 TO JUNE 1978.

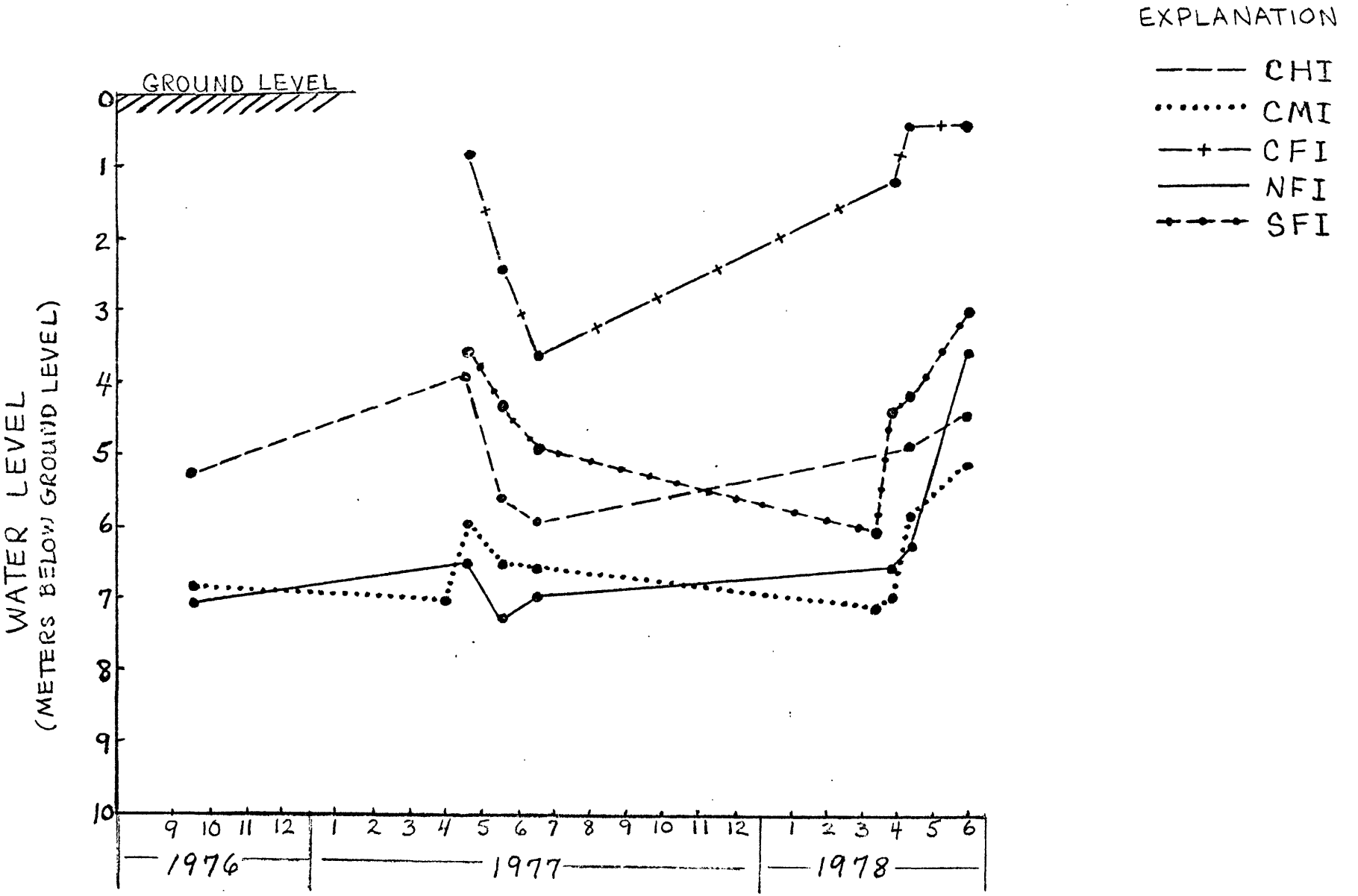

FIGURE 10: WATER LEVELS MEASURED IN INCLINOMETER HOLES FOR SEPTEMBER 1976 TO JUNE 1978.

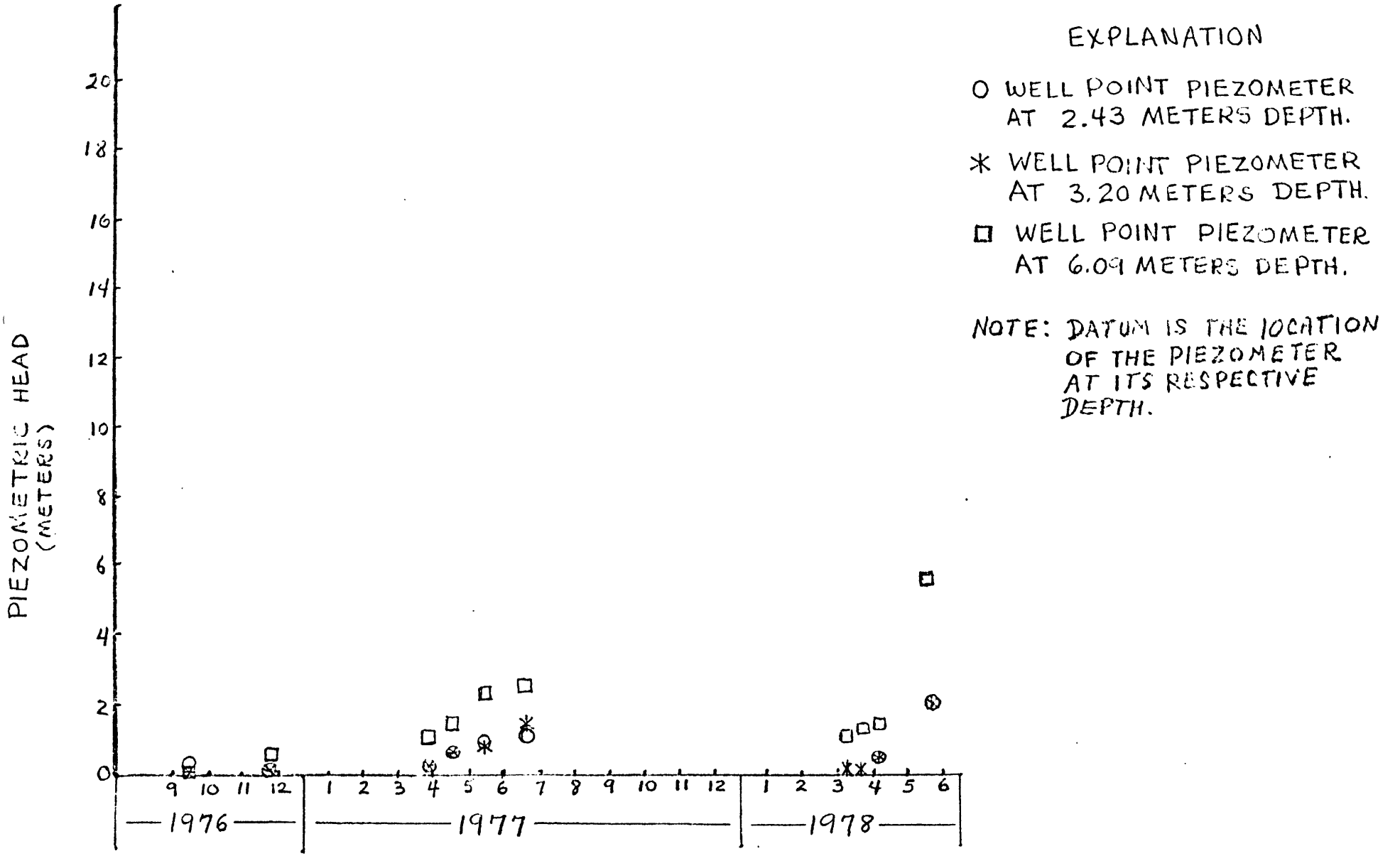

FIGURE 11: VARIATION IN PIEZOMETRIC HEAD AT THREE MEASURING POINTS IN DRILLHOLE NOW 17 METERS NORTH OF THE SLIDE FOR SEPTEMBER 1976 TO JUNE 1978.

GEOTECHNICAL LOGS

Logs relating incremental displacement changes detected by the inclinometer to lithologies, pocket-penetrometer values, and hydrochloric acid reaction are presented in figures 12-15. Incremental displacement changes rather than the cumulative profiles were used to accentuate zones of movement. The values were calculated for each measuring point in the profile by subtracting displacements measured April 4, 1978, from initial values (fall 1976). Lithologic descriptions for boreholes CMI and CFI are based on field logs by Ebaugh (1977) supplemented by the author after microscopic examination.

General Description of Materials

As shown in the logs, drill-hole lithologies are predominantly silty clay with occasional thin zones or beds of carbonaceous clay and fine to coarse sand. Although most of the materials are soil-like, some of the deeper, relatively unweathered materials are well indurated (penetrometer indices >5) and are properly described with rock names.

Chemical weathering, manifested by iron oxide stain, calcium carbonate accumulations, and secondary gypsum (selenite) crystals, was observed in core sample from as deep as 15 m--the depth of the deepest hole drilled. In general, the abundance of those indicators decreases with depth; however, such things as composition of the material, the presence or absence of interbedded aquifers, and small-scale discontinuities greatly influence the location, degree, and nature of chemical weathering within the slope. Concentrations of gypsum crystals, for example, tend to occur in clay zones in association with carbonaceous material.

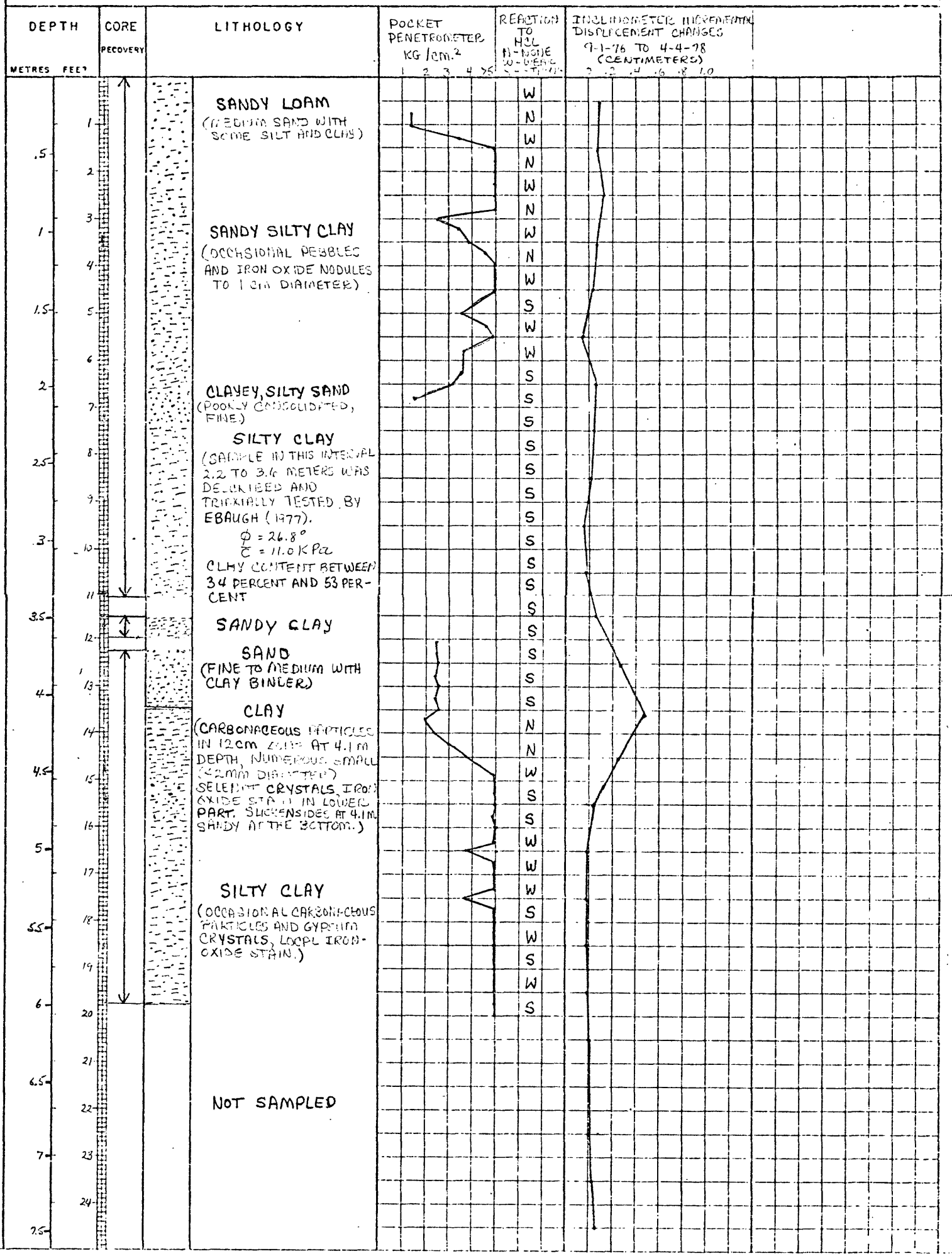

FIGURE 12: GEOTECHNICAL LOG FOR THE CENTER HEAD INCLINOMETER HOLE (CHI).

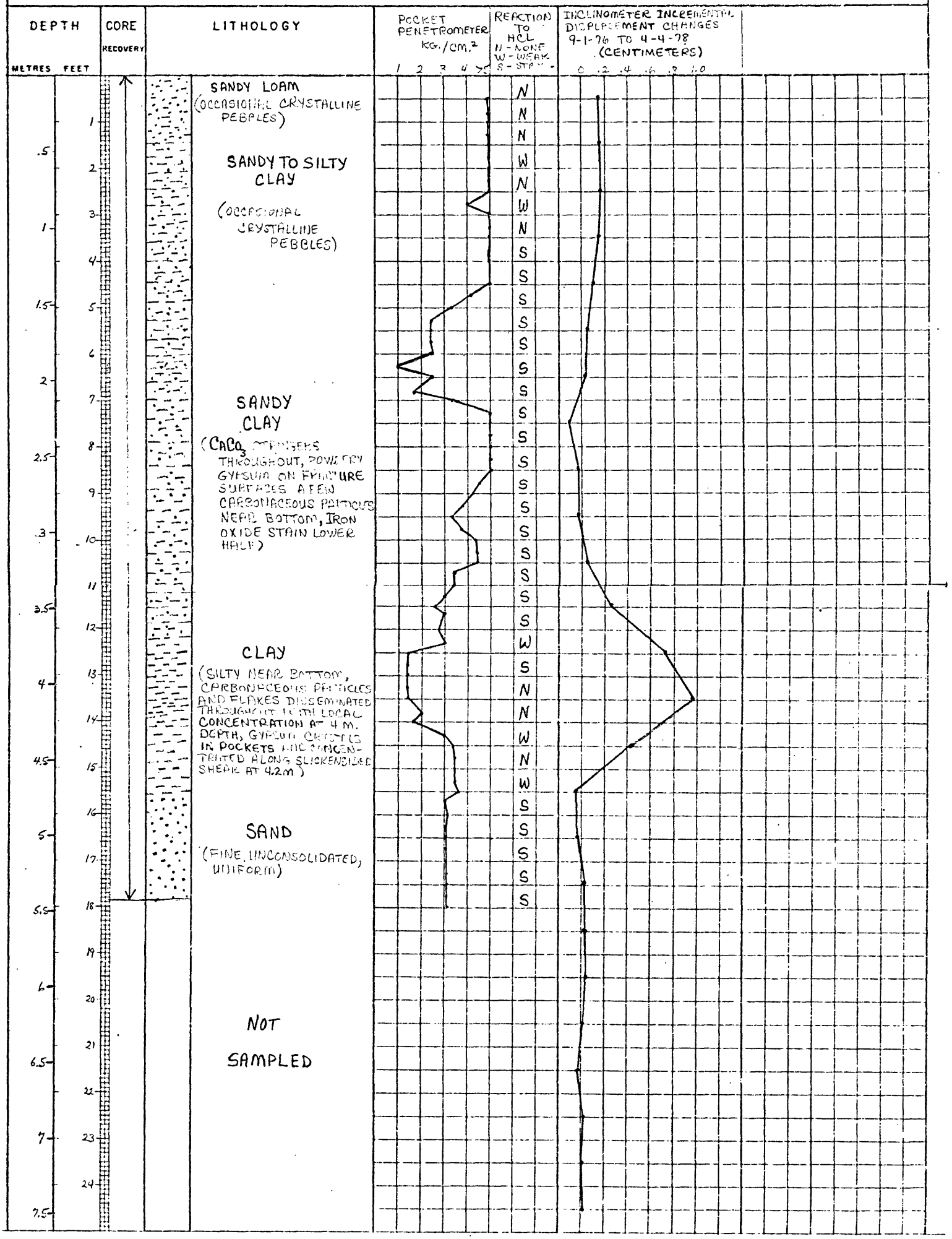

FIGURE 13: GEOTECHNICAL LOG FOR THE NORTH FLANK INCLINOMETER HOLE (NFI).

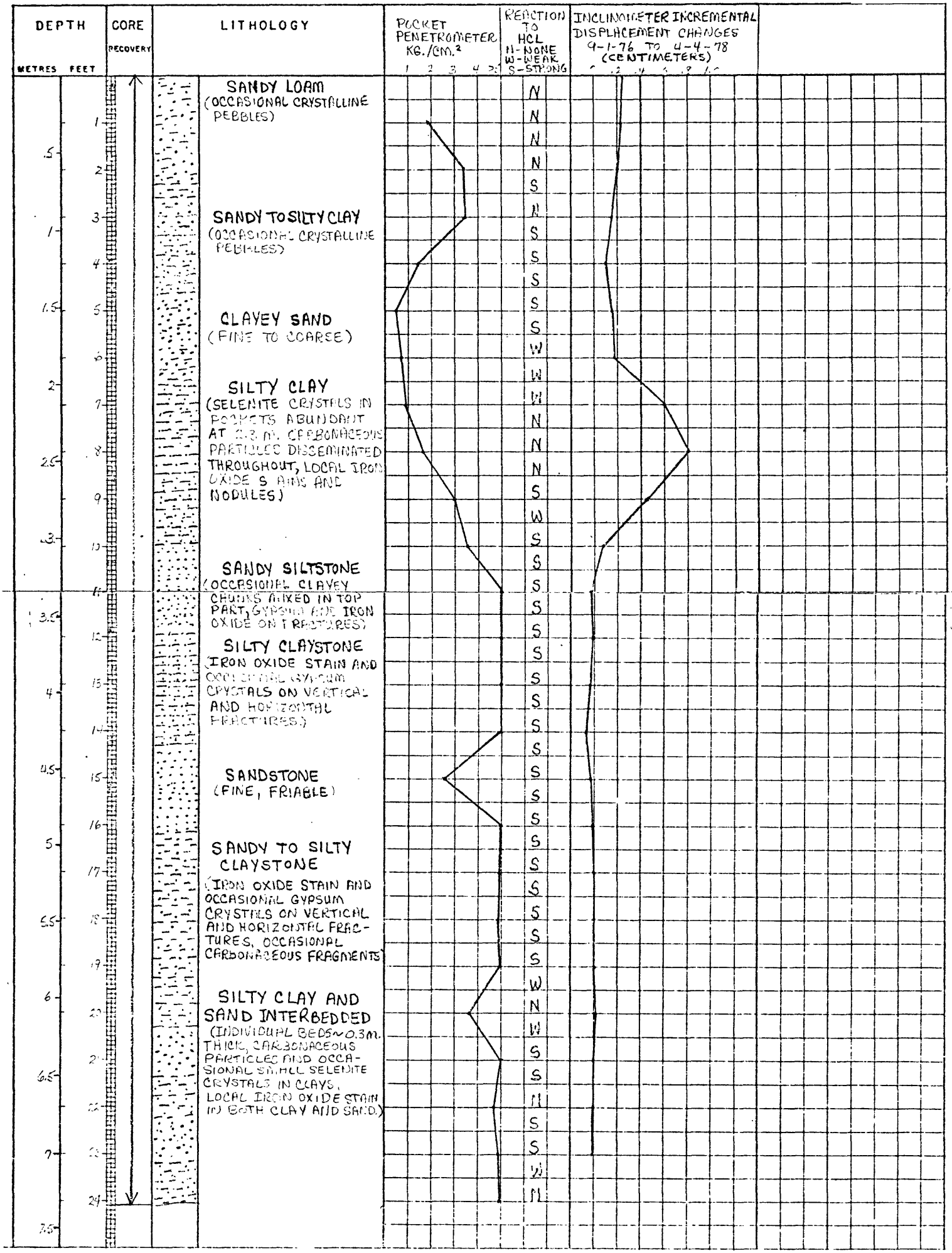

FIGURE 14: GEOTECHNICAL LOG FOR THE CENTER MIDDLE INCLINOMETER HOLE (CMI).

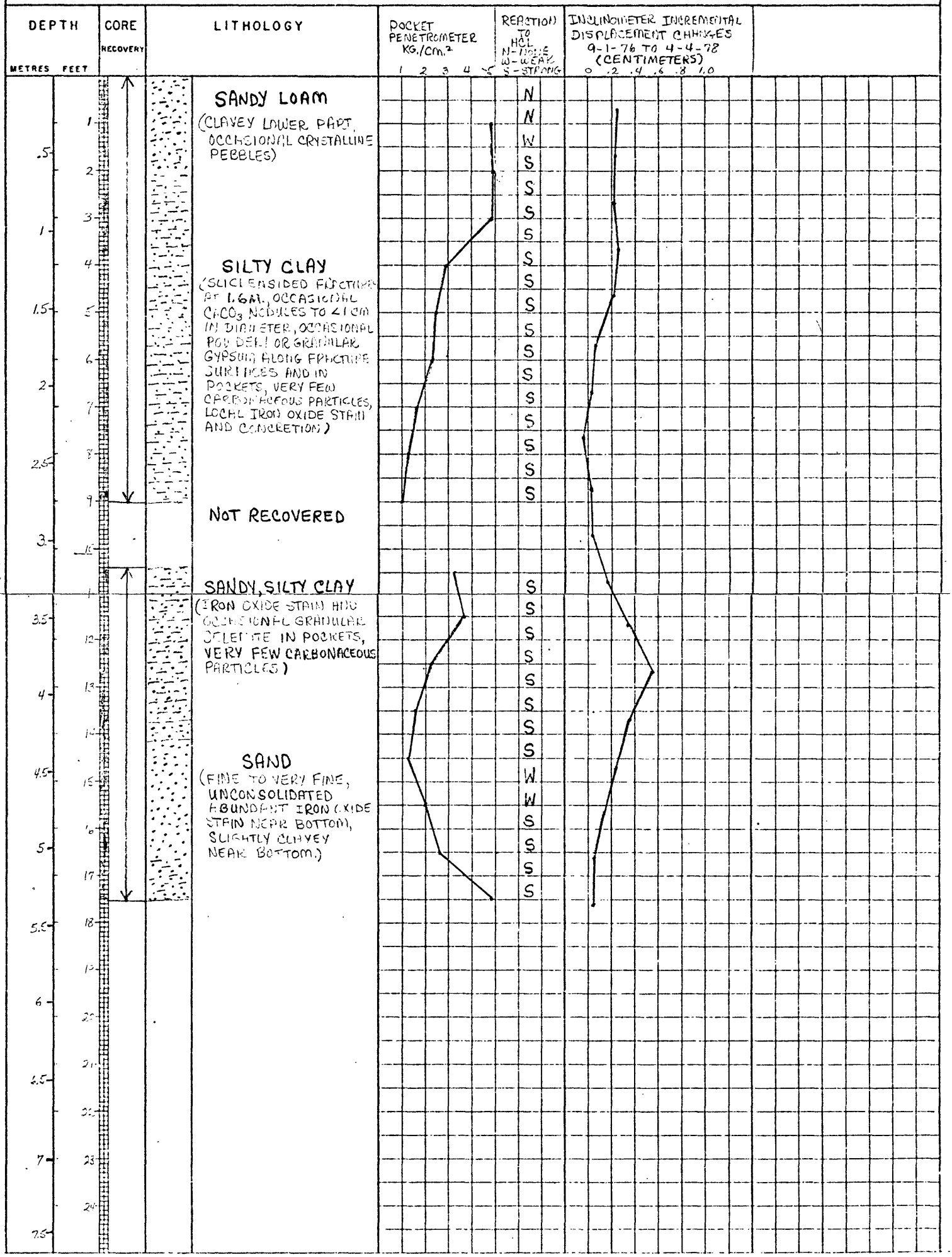

FIGURE 15: GEOTECHNICAL LOG FOR THE CENTER FOOT INCLINOMETER HOLE (CFI).

During field examination of the core sample, slickensided shear were observed at 1.6-m depth at the foot of the slide (CFI) and at 13-m depth at the head of the slide in piezometer-hole CHP. The latter appears unrelated to the slide movement detected by the inclinometer. The slickensides at 1.6 m in CFI are oriented at 20° from the horizontal. Although they are very near the lower limit of the zone of surface creep, they are probably the result of shearing during the initial failure. Striations indicating displacement were noted on the slickensided surface. The top 5 cm of a thin siltstone bed, 3.3 m deep at the middle of the slide (CMI), was fractured, and mixing of clayey chunks with the siltstone was noted. Fissures were noted in near-surface material from all the boreholes and are probably the result of desiccation, frost action, and thermal expansion. A few joints were observed in core samples from the deeper, relatively unweathered parts of the drill holes.

Description of Material from the Zones of Movement

Material from zones of maximum displacement in the lower zones of movement of inclinometer holes CHI, NFI, and CMI (figs. 12-14) can be characterized as follows: clay rich with conspicuous amounts of carbonaceous particles occurring as specks and flakes desseminated throughout the clay or concentrated in thin zones along bedding planes, and gypsum (selenite) that occurs as small disk-shaped crystals in pockets in the clay or along the slickensided horizontal fractures (fig. 16). Additionally, they are zones low in carbonate content as indicated by their reaction to hydrochloric acid.

Figure 16. Photograph of Shelby tube core sample (7-cm diameter) from the lower zone of movement in inclinometer-hole NFI. The figure shows slickensided horizontal shear with gypsum crystals.

Detailed examination of the core sample in the laboratory revealed throughgoing slickensides at the points of maximum displacement in inclinometer-holes CHI (4.2 m) and NFI (4.2 m). In inclinometer-hole NFI the slickensides are horizontal and show faint striations indicating displacement (fig. 17). Orientation of the majority of the crystals parallel with the slickensided surface and the presence of sheared and ground crystals, often mixed with the clay, also indicate displacement and establish the presence of most of the crystals prior to some or all of the movement. Throughgoing slickensides were not found in samples from the middle of the slide (CMI). However, a few local slickensides were observed in silty clay from the lower zone of movement. These were small and slightly curved, and appeared randomly oriented.

The lower zone of movement in inclinometer hole CFI, at the foot of the slide, involved a sandy, silty clay and an unconsolidated fine sand that have relatively high carbonate content and very little gypsum or carbonaceous material.

Movement in the zone of surface creep does not appear to have corresponded to a definable lithologic unit or soil horizon. Although colluvial material is involved, movement in the upper zone appeared to extend beneath the colluvium into in-place material below. The colluvial layer is poorly defined and often the only indicator that helps distinguish it from weathered material immediately below is the presence of crystalline pebbles that are known to originate at the surface. The low-carbonate content of the material near the surface can be accounted for by leaching action of infiltrating surface water. Accumulation of $CaCO_3$ below the leached zone is indicated by the strong acid reaction shown in the logs (figs. 12-15).

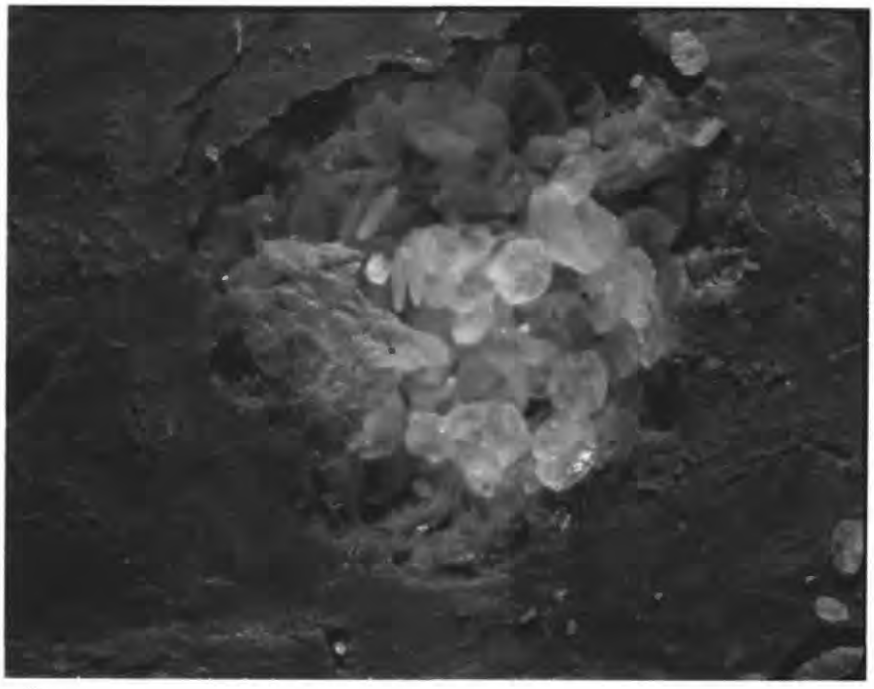

Figure 17. Microphotograph of a small area of the slickensided shear surface shown in figure 16. The photo shows a sheared pocket of gypsum crystals. Magnification is 15X.

Intervals of low pocket-penetrometer values only roughly correspond to zones of movement in the profiles. Penetrometer values are relatively high in the top meter or so. Because sampling was done during the dry time of year, the high values can probably be accounted for by low-moisture contents resulting from surface evaporation, which tends to harden and strengthen the clayey material.

LABORATORY TESTING

X-ray and Chemical Analyses

X-ray and chemical analyses were performed on samples from 3.6 to 6.2 m in inclinometer-hole CHI to determine clay types and abundance and to examine changes in mineralogy with depth across the zone of movement and into the immobile material below. Chemical analyses to measure total carbon and total sulfur content were performed on the same samples to determine the abundance of carbonaceous material and, in conjunction with the X-ray analyses, to estimate amounts of organic carbon and sulfur. Part of the tested core sample (that from the lower zone of movement) is shown in figure 18. Results of the analyses are presented in figure 19.

Relative abundance with depth of gypsum, dolomite, calcite, and quartz is indicated by X-ray peak heights. It can be seen that the zone of maximum displacement between 4.1 and 4.3 m is high in gypsum, low in quartz, and very low in carbonate content relative to material above and below. The conspicuous change in composition at 4.2 m in figure 19 corresponds to the "carbonaceous" clay with gypsum crystals shown in figure 18. Increases in quartz content above and below the zone are associated with the yellow clayey sand above 4.1 m and with silty material below 4.3 m depth.

page 35 follows

Figure 18. Photograph of Shelby tube core sample from the lower zone of movement in inclinometer hole CHI (3.9-4.5 m). Black specks in the core are carbonaceous particles in clay. White specks are gypsum crystals.

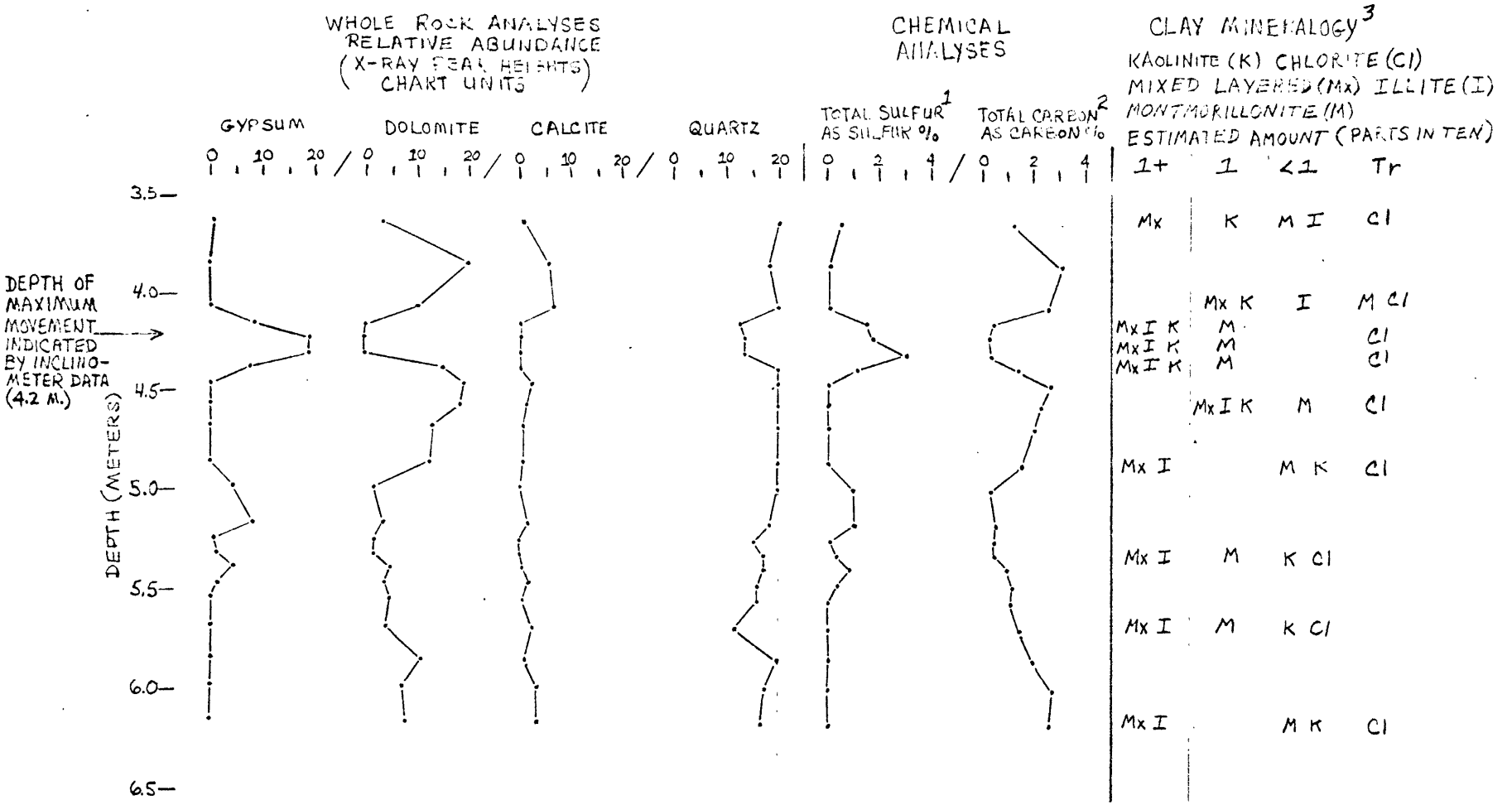

FIG. 19 -- X-RAY AND CHEMICAL ANALYSES OF SAMPLE FROM INCLINOMETER HOLE CHI, SHOWING CHANGES IN MINERALOGY, TOTAL SULFUR, AND TOTAL CARBON CONTENT IN RELATION TO DEPTH.

Tr = Trace = < 5 percent
<1 = 5-9 percent

1 Analyses by P.H. Briggs
2 Analyses by V.E. Shaw
3 Analyses by Paul D. Blackmon

Total carbon and total sulfur percentages include both mineral and organic sources. The low values of total carbon between 4.1 and 4.3 m reflect the low carbonate content shown in the X-ray analyses and indicate that the amount of carbonaceous material, though conspicuous in the core sample, is not greater than 0.5 percent. Total sulfur percentages, as expected, are high in zones of high gypsum content. Because sulfides such as pyrite are absent, or nearly so (did not give measureable peak heights), and the total carbon content of the samples is very low (implying low organic sulfur as well as low organic carbon), it is assumed that most of the sulfur content results from the sulfate of the gypsum.

A well-documented weathering phenomenon, which may account for the high gypsum content in the clay, was described by Krauskopf (1967). In the zone of weathering, oxidation of sulfides to sulfates is commonplace. The chemical reaction $2FeS_2+15/2\ O_2-4H_2O\ \ Fe_2O_3+4SO_4\ +8H^+$, locally catalyzed by bacteria, can result in saturation of the environment with sulfate ions that combine with available calcium ions to form gypsum. It is not known if sulfides were originally present in sufficient quantity to support the process; however, low sulfide contents would be expected in weathered zones where the reaction has neared completion.

Clay minerals present include montmorillonite-illite mixed layer, illite, kaolinite, montmorillonite, and chlorite. Total clay content is highest in the zone of maximum displacement where mixed-layer, illite, kaolinite, and montmorillonite clays are present in nearly equal amounts. Clay-size quartz and feldspar account for the difference between the clay-size contents shown in table 1 and the total clay mineral content indicated in figure 19.

Strength and Physical-Property Testing

As previously mentioned, Ebaugh (1977) triaxially tested silty clay samples of slide material (the main soil type in the slide) from 2.2 to 2.6 m depth from inclinometer-hole CHI. Inclinometer data (fig. 12) has since shown that the material tested was above the lower zone of movement in the rigid zone of the displacement profile. In an effort to determine strength properties of materials similar to those found in the zone of movement, consolidated drained direct-shear tests were run on Shelby tube core sample of weathered carbonaceous clay from borehole NOW, 17 m north of the slide. The material was similar in composition and weathering characteristics to that found in the lower zone of movement in inclinometer holes CHI, NFI, and CMI. Additionally, for purposes of comparison, core sample of stiff, silty clay from the immobile zone of inclinometer hole CHI was tested in direct shear. Because of limited sample, the single sample from borehole NOW was multistage strength tested (Kim and Ko, 1977) to obtain peak strengths at differing normal loads, from which a strength envelope could be drawn (fig. 20). Coefficients of consolidation were determined prior to testing in order to ascertain strain rates necessary to eliminate pore pressure buildup during testing (Bishop and Henkel, 1957).

In conjunction with the strength tests, Atterberg and size analyses were performed on the shear-test samples. Atterberg and size analyses were also performed on material from the lower zone of movement from inclinometer holes CHI and NFI. Test results are presented in figure 21 and in table 1. Triaxial test results from Ebaugh (1977) are included in table 1 for comparison.

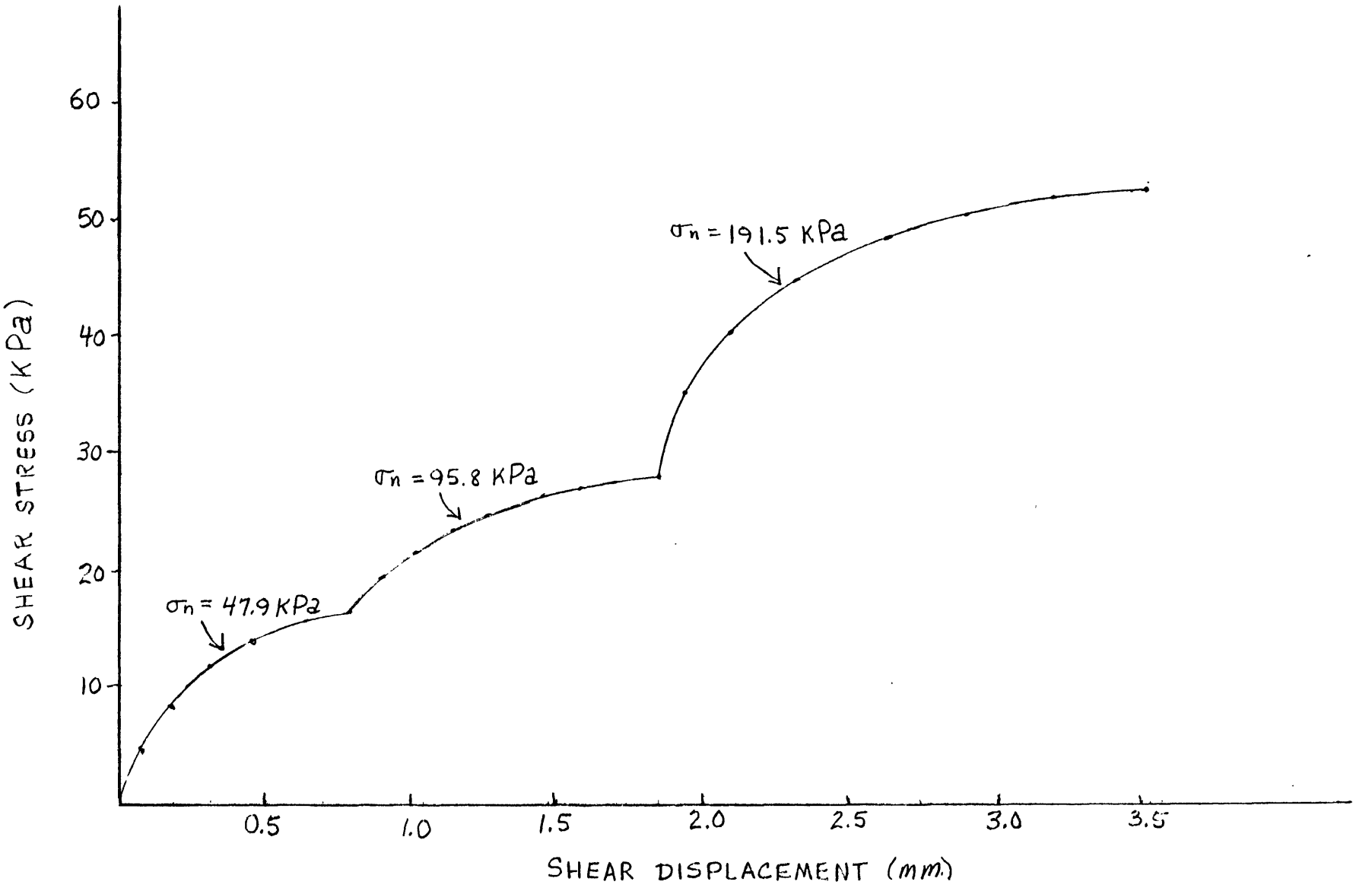

FIGURE 20: RESULT OF MULTI-STAGE CONSOLIDATED-DRAINED DIRECT SHEAR TEST OF A SINGLE SAMPLE (NOW 2.26 M.) USING GRADUATED NORMAL LOAD (σ_n) INCREMENTS OF 47.9 KPa, 95.8 KPa, AND 191.5 KPa.

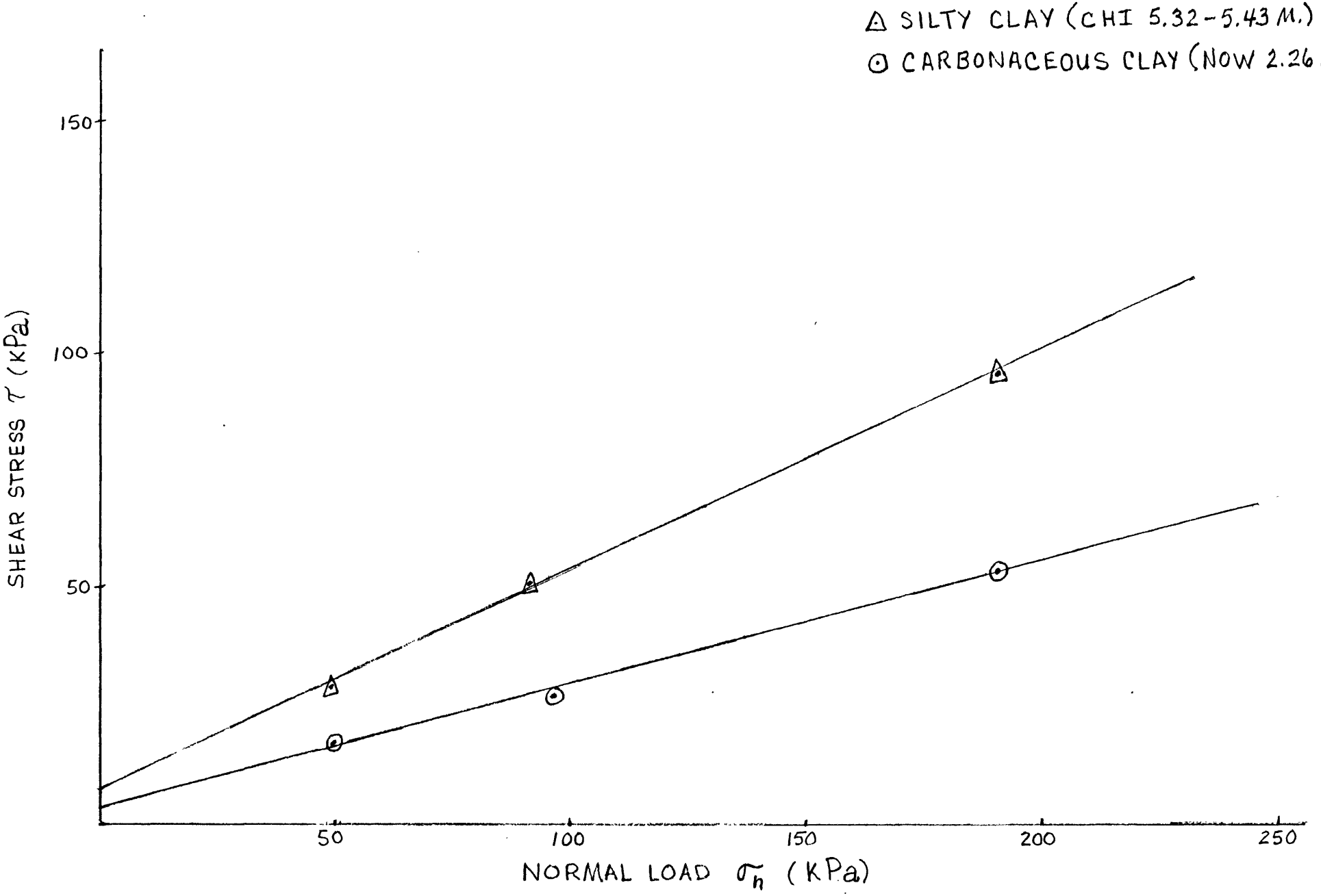

FIGURE 21 : MOHR ENVELOPES FOR WEATHERED CARBONACEOUS CLAY AND SILTY CLAY.

Table 1.--Strength parameters, physical properties, and composition of selected samples

Drill hole	Depth (meters)	Location	Peak strength parameters shear stress at failure σ_n = 96 kPa			Atterberg limits			Natural moisture content	Clay content (<2μ)
			kPa	C (kPa)	ϕ (deg)	PL	LL	PI	(percent)	(percent)
				Carbonaceous clay with gypsum crystals						
CHI	4.20	Lower zone of movement	---	---	---	26	86	60	37	95
NFI	4.22	Lower zone of movement	---	---	---	27	88	61	35	92
NOW	2.26	Off-slide drill hole	28[1]	3[1]	15[1]	32	90	58	39	94
				Silty clay						
CHI	5.22	Immobile zone (beneath slide)	---	---	---	24	70	46	24	85
CHI	5.32	--do----				23	72	49	24	85
CHI	5.37	--do----	52[1]	7[1]	25[1]	22	74	52	22	83
CHI	5.43	--do----				25	62	37	26	79
CHI	2.20-3.70	Rigid zone within slide (Ebaugh, 1977)	---	11[2]	27[2]	23[3]	52[3]	28[3]	---	44[3]

[1]Determined by consolidated-drained direct shear test.

[2]Determined by consolidated-drained triaxial tests.

[3]Average of four samples tested.

The Atterberg limits reflect the clay proportions in the samples. Note the similarity between shear-tested off-slide sample NOW (2.26 m) and samples CHI (4.20 m) and NFI (4.20 m) from the zone of movement. The triaxially tested silty clay from the rigid zone shown in the movement profiles (fig. 3), is the lowest in clay content and limits. Measured natural-moisture contents of all the samples are at or above the plastic limit but are highest for the carbonaceous clays.

Strength parameters of the carbonaceous clay are significantly lower than either the silty clay from beneath the lower zone of movement or that from the rigid zone above.

CLIMATIC EFFECTS

Graphs of weather data compiled by the Sheridan weather station, showing daily temperature, precipitation, and snow conditions during, before, and after periods of significant slide movement during the spring of 1977 and 1978, are presented in figures 22 and 23. It can be seen from the daily temperature graphs that the movements occurred during warming trends in early April 1977 and late March and early April 1978 when minimum temperatures were generally at or above freezing. Precipitation, mostly in the form of snow between March 24 and April 4, 1977, accumulated to a depth of 0.27 m. Because of drifting, snow accumulation was much greater on the landslide, reaching a depth at the head of a little more than 2 m on April 2. Subsequent snowmelt and thaw coincided with the period of movement (shaded area) shown in figure 22. Precipitation just prior to movement in the spring of 1978 was negligible (fig. 23); however, snow accumulation from previous storms remained. Once again, the accumulation on the landslide was considerably more because of drifting (2 m at the head of the slide on March 13). Consequently, the Sheridan weather station reported trace amounts remaining on the ground by March 24, whereas 1-1.3 m remained on the landslide. As in early April 1977, movement in late March and early April 1978 coincided with snowmelt and spring thaw. The unusually heavy rains of mid-May 1978 triggered many new landslides in the Sheridan area and reactivated some existing slides. At the site, the average water levels and pore pressures were the highest of any measured during the 1-1/2-year study period (figs. 9-11) and resulted in several inches of renewed sliding.

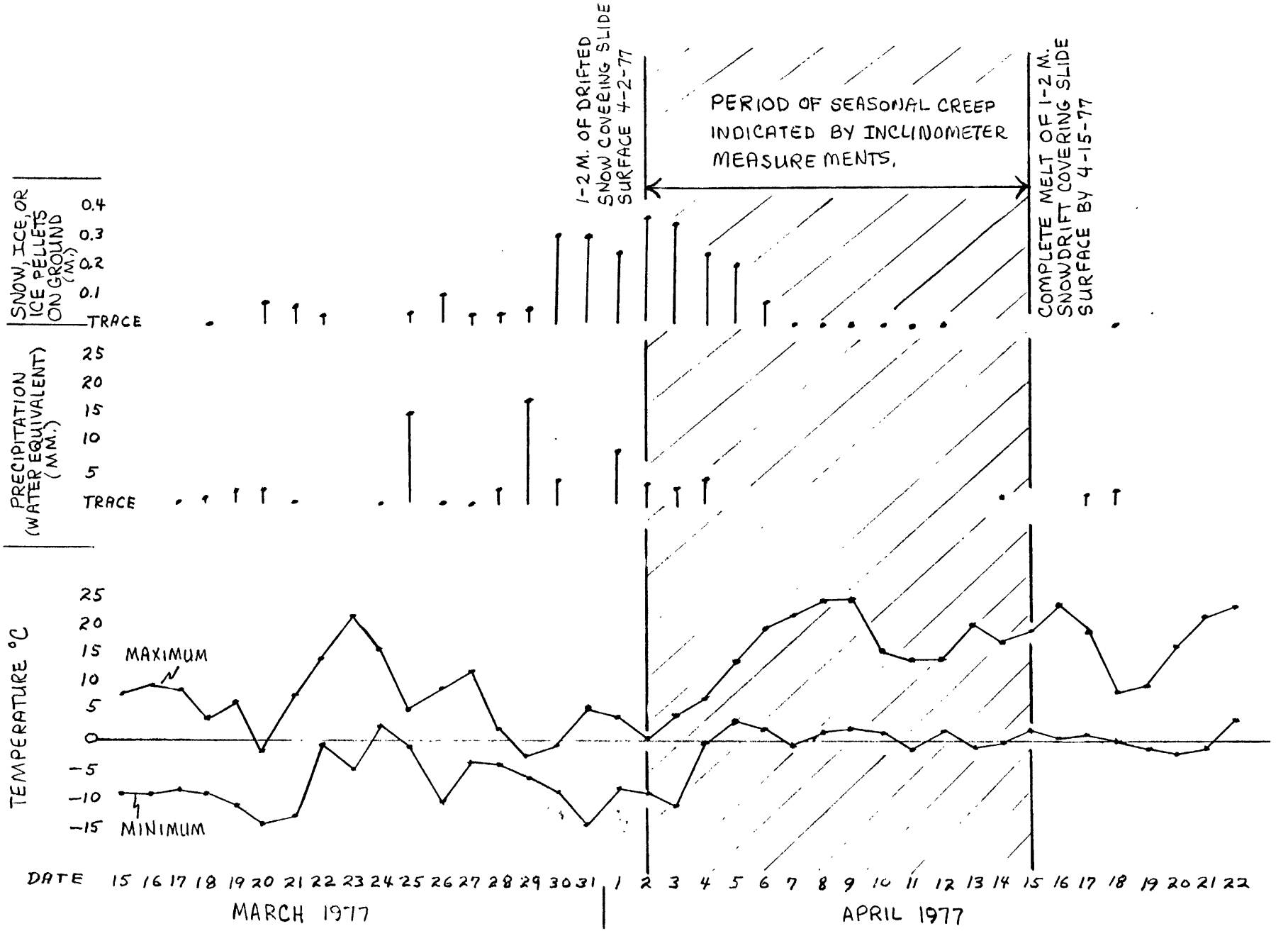

FIGURE 22: GRAPHS SHOWING DAILY TEMPERATURE MAXIMUMS AND MINIMUMS, PRECIPITATION, AND SNOW OR ICE ON GROUND AT THE SHERIDAN, WYOMING WEATHER STATION DURING THE PERIOD MARCH 15, 1977 TO APRIL 22, 1977 (NATIONAL CLIMATIC CENTER, 1977), AND THEIR RELATION TO RECORDED SLIDE MOVEMENT AND SNOWMELT BETWEEN APRIL 2, 1977 AND APRIL 15, 1977.

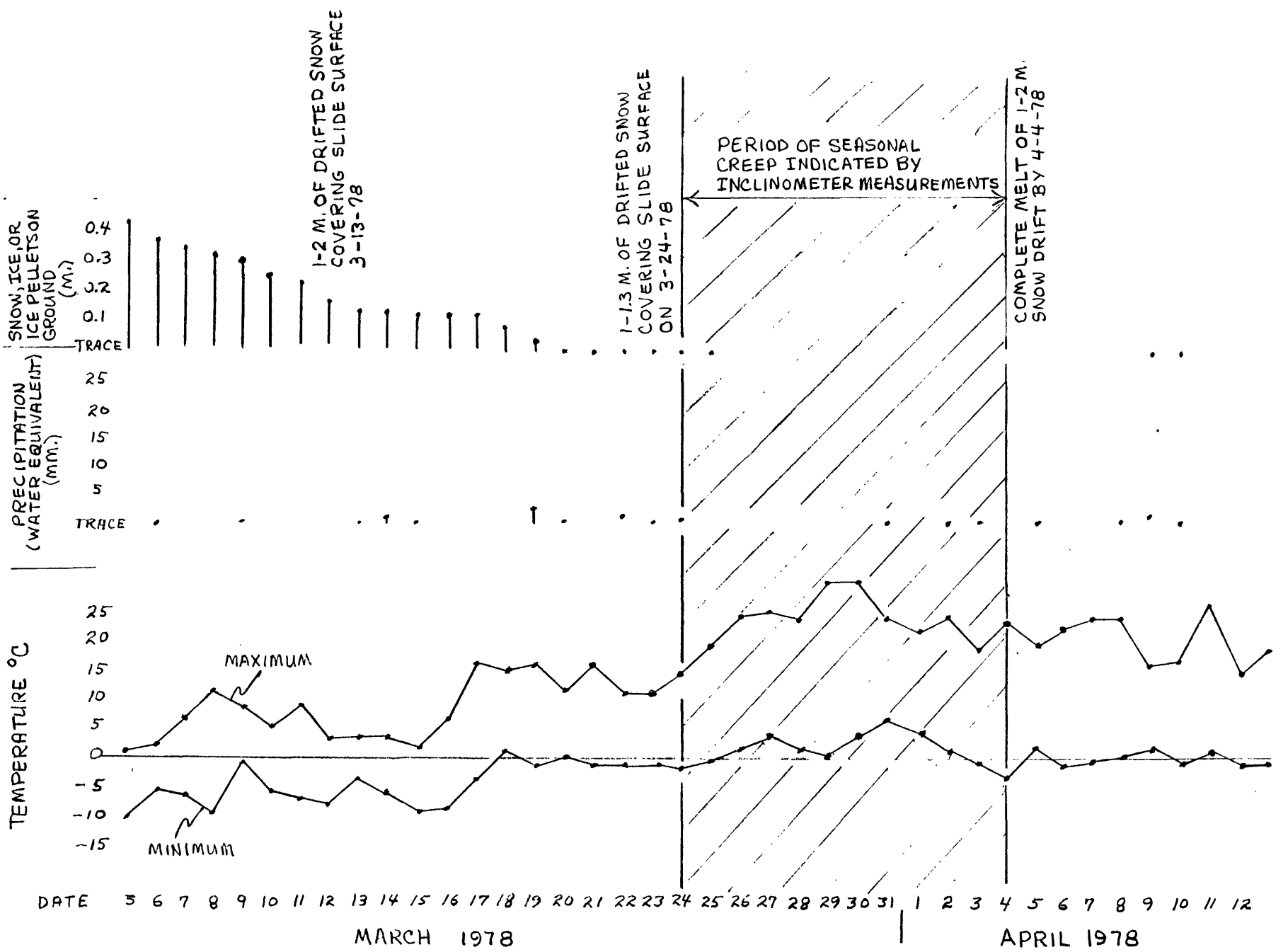

FIGURE 23: GRAPHS SHOWING DAILY TEMPERATURE MAXIMUMS AND MINIMUMS, PRECIPITATION, AND SNOW OR ICE ON GROUND AT THE SHERIDAN, WYOMING WEATHER STATION DURING THE PERIOD MARCH 5, 1978 TO APRIL 4, 1978 (NATIONAL CLIMATIC CENTER, 1978), AND THEIR RELATION TO RECORDED SLIDE MOVEMENT AND SNOWMELT BETWEEN MARCH 24, 1978 AND APRIL 4, 1978.

DISCUSSION

Nature of the Initial Failure

The exact date of the initial failure is unknown, but, according to the landowner, it occurred in late spring 1973 after a heavy snowstorm. Aerial photographs of the site taken in July 1966 show no indication of failure. Precipitation records of the National Climatic Center (1974) indicate 102 mm of precipitation for the month of April 1973, mostly in the form of snow, whereas 53 mm is average. Seasonal creep deformation of the slope similar to that detected by the inclinometer measurements may have conditioned the slope prior to the sudden failure. Slope failures are commonly preceded by creep deformation near the surface and within the slope, and landslides that develop from seasonal creep may continue to creep after major movement (Terzaghi, 1950). Although no evidence of older sliding was observed at the site, the low slope angle and indications of older slides in adjacent areas suggests the possibility that lower than peak strengths have been mobilized.

The probable extent of the initial failure (spring 1973) is shown in cross section in figure 24. The failure limits are based on surface indications, inclinometer data, and the geotechnical logs. The orientation and location of the failure surface suggests both lithostratigraphic and weathering controls. Lithostratigraphic control appears dominant in those areas where the dip of the failure surface most nearly approximates the shallow dip of the beds (1° NE). According to inclinometer data, laboratory test data, and logging information, the control is imparted by weak but thin and discontinuous carbonaceous clay zones. Weathering control is suggested by signs of intense weathering in the zones of movement, chiefly iron oxide stain and concentrations of gypsum crystals. Additionally, the previously mentioned seismic survey by Miller (1979) defined a low-velocity layer of relatively low strength that included the landslide and extended to a depth that coincides with what was described as a subweathered transitional zone between weathered and relatively unweathered bedrock. It was found that the low-velocity layer nearly parallels the restored topographic slide surface. Consequently, weathering control may be dominant where the failure surface most nearly parallels the slope (12°). The combined effect of these and other factors was an undulating failure with translation at the head and middle of the slide and flow at the foot where the water content was highest and some lateral spreading was evident.

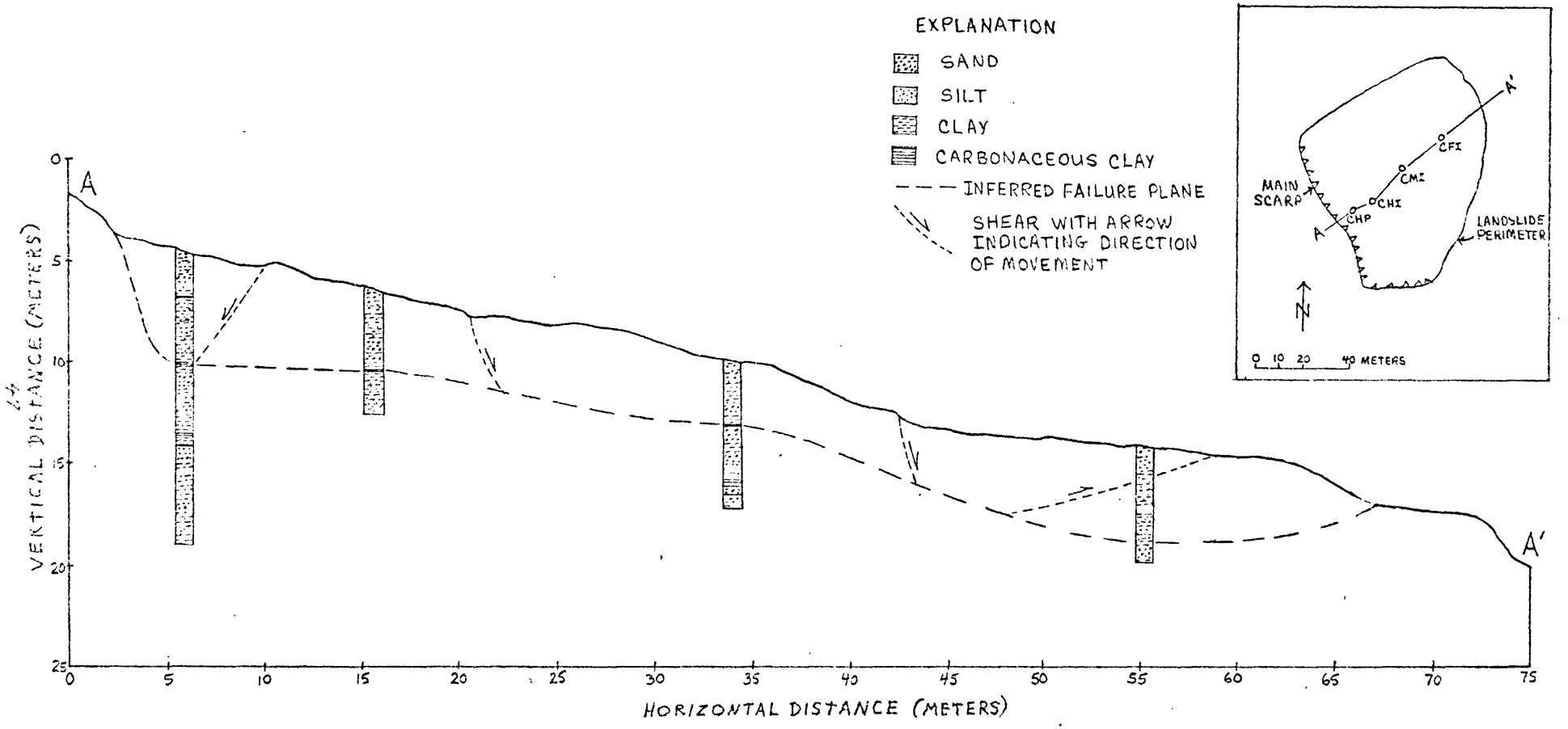

FIGURE 24: LANDSLIDE CROSS SECTION SHOWING INFERRED FAILURE SURFACE, SHEARS, AND DRILL HOLE LITHOLOGIES. DRILLHOLE DIAMETERS ARE EXAGGERATED FOR THE PURPOSE OF ILLUSTRATION.

High pore pressure at the head of the slide (5.3-m depth), resulting from a perched water table, probably contributed to but may not have been necessary for failure. The low-strength parameters associated with the carbonaceous clay zones were used in an infinite slope analysis similar to that used by Ebaugh (1977) for the triaxially tested silty clay. The analysis (Lambe and Whitman, 1969), which models a saturated slope condition (water table at or near the surface) without artesian water pressures, relates slope angle and depth to failure in the following equation of limiting equilibrium:

$$\frac{C}{\gamma_t H_c} = \cos i \, (\tan i - \frac{\gamma_b}{\gamma_t} (\tan \phi)$$

where:

i = slope angle

H_c = depth to failure surface

C = cohesion

ϕ = internal friction angle

γ_t = total unit weight

and γ_b = buoyant unit weight.

The result of the analyses shown in figure 25 indicates that failure was possible on slopes as gentle as 10° at approximately 3.5 m depth (the average depth of the actual failure), assuming strength properties along the failure plane similar to those of the strength tested carbonaceous clay. Curves generated by using the strength properties of the silty clays are shown for comparison.

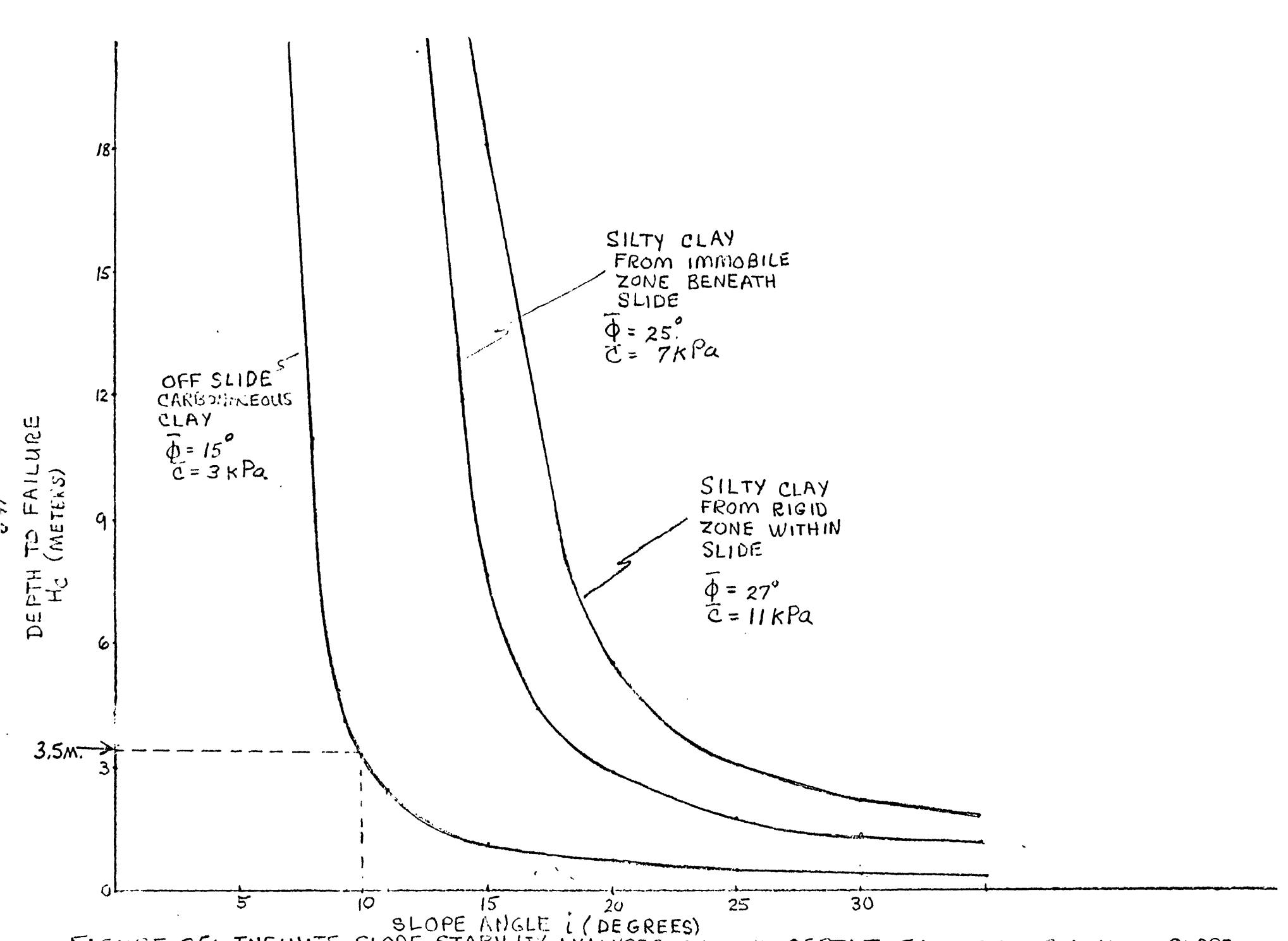

FIGURE 25: INFINITE SLOPE STABILITY ANALYSES SHOWING DEPTH TO FAILURE FOR VARIOUS SLOPE ANGLES. THE ARROW AND DASHED HORIZONTAL LINE MARK THE AVERAGE DEPTH AT

Creep movements

The term "creep" is used to describe slow downhill movement that is usually imperceptible except to long-term observations (Sharpe, 1938). Initiation of soil creep by ground water resulting from the percolation of rain or melting snow has been reported by Fukuoka (1953) in Japan.

Creep-deformation profiles similar to those of this report were predicted and measured by Ter-Stepanian (1965) on the Black Sea coast of the Caucasus (fig. 26). Ter-Stepanian (1965) interpreted the displacement profile of figure 26 as follows: (1) a curvilinear section M'P' in the zone of surface creep; (2) vertical section P'Q' in the zone of rigid displacement; (3) curvilinear section Q'R in the zone of depth creep and vertical section RN in immobile rocks. Creep movement in the zone of depth creep is interpreted as a viscous flow phenomenon near potential planar or circular-cylindrical sliding surfaces. The rate of creep deformations and the thickness of the creep zone change with a change in intensity of landslide-producing factors, such as the height of the piezometric level.

Creep in the upper zone of movement of the landslide may be related to frost penetration. Kirkby (1967) used seasonal freeze and thaw and the downhill gravity component to account for certain creep phenomenon. The average depth of frost penetration in the Sheridan area is between 0.76 and 1.02 m, although extreme frost may extend to 1.5 m. These depths correspond to the depth of surface creep indicated in the displacement profiles. Other possible causes of surface creep, such as variations in soil moisture, also need to be considered.

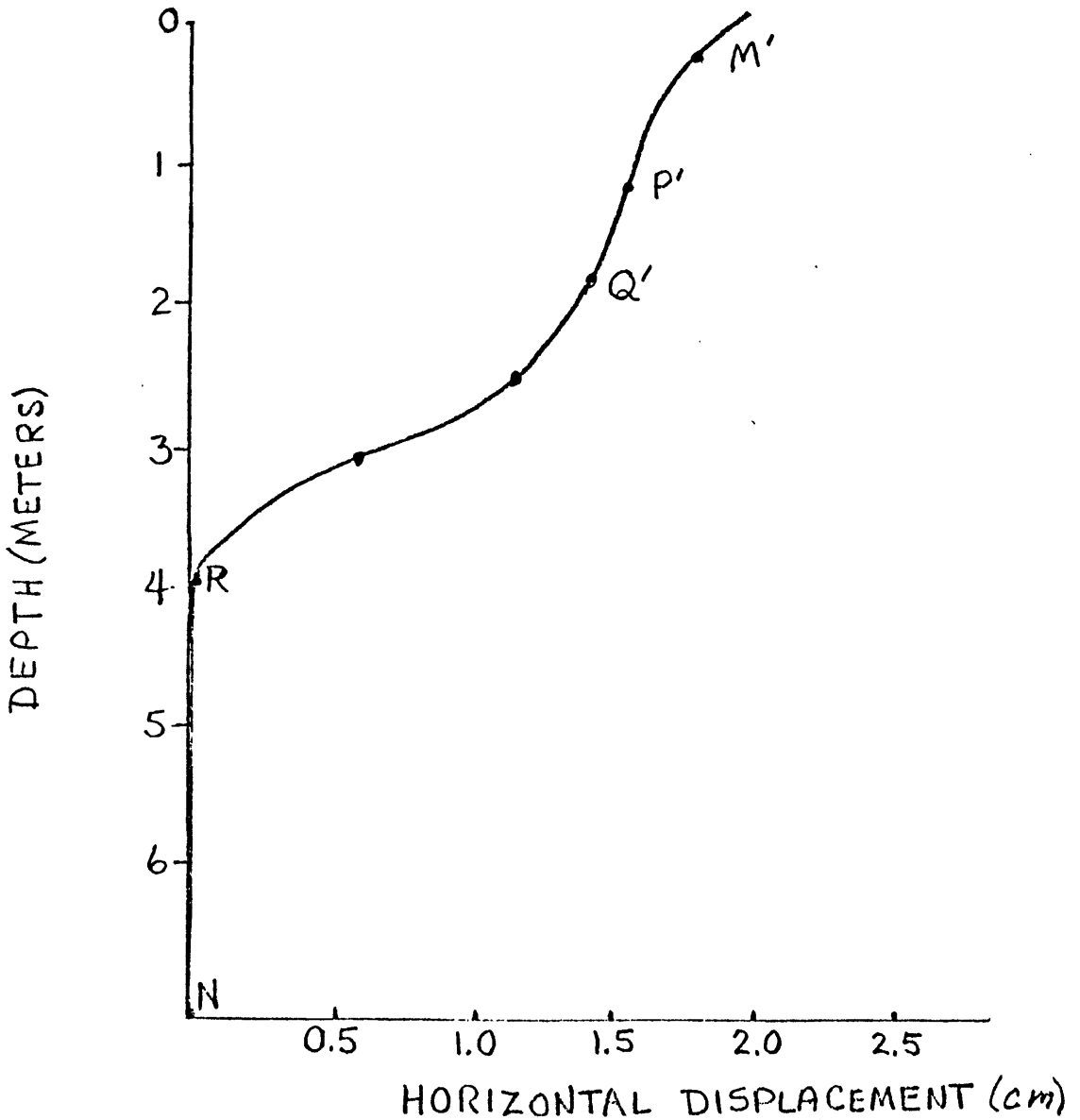

FIGURE 26: CREEP DEFORMATION PROFILE FOR LANDSLIDE SLOPES OF THE BLACK SEA COAST OF THE CAUCASUS (TER-STEPANIAN, 1965).

COMPOSITION AND WEATHERING EFFECTS

Four different clay types are present in the failure zone in appreciable amounts (fig. 19), however, their individual significance is uncertain. Booy (1978) compared material from slope failures in various parts of northern and central Wyoming, including slides a few miles south of the study slide, which were found to contain major smectite and kaolinite and minor illite. Atterberg limits and shear strengths higher than those of materials involved in other nearby earth flows, but comparable to those of true bentonite slides in other areas, were attributed to the fine particle size and mineralogical composition of the failed material.

Carbonaceous zones typically have high moisture contents and appear to act as aquifers that possibly wet nearby clays, changing their physical properties and enhancing the weathering process. The weathering of carbonaceous material may introduce organic ions which affect the plasticity of certain clays through ion exchange. Some organic materials are thought to increase plasticity, as with the Ball clays (Grim, 1962).

The significance of the weathering process that gives rise to secondary gypsum in certain unstable slopes is poorly understood. Tchourinov (1945) investigated weathering effects in Cretaceous sediments along the Volga and Sviaga Rivers, Russia, in an area where landslides are closely related to the weathered zone. Alteration due to weathering resulted in gypsum replacing marcasite in black clay containing finely divided organic material. The structure of the weathered clay was less compact than equivalent unweathered material, and microscopic fissures had developed. Chemical analysis of altered and unaltered clays indicated that weathering resulted in an increase in sulfates, an increase of calcium and magnesium ions, no significant change in sodium content, and a decrease in the quantity of organic matter. Physical-property and strength testing showed an increase in porosity and moisture content, reduced Atterberg limits, and decreased strength and cohesion for the altered clays. Tchourinov concluded that the alteration of the clays should be considered a main cause of landsliding. Eardley and Stringham (1952) described selenite that occurs in pockets in highly plastic sodium clays near the shore of the Great Salt Lake. According to these authors, the discovery of selenite crystals in the Great Salt Lake clays was unexpected because gypsum or anhydrite has never been precipitated on the lake bottom, as the lake waters are impoverished in calcium ions because of copious precipitation of $CaCO_3$. It was suggested that physical changes resulting from the consolidation process might account for excess calcium ions detected in the pore water of the clay. The (010) main cleavage face of the Great Salt Lake selenite crystals were found to be perpendicular to the flat dimension of tabular shape of the crystals, contrary to common occurrences in which the (010) face is parallel to the flat dimension. They theorized that the unusual shape suggested a process of recrystallization after original growth and that

stresses related to plastic flow or compaction might account for the shape of the unique crystals. It is of interest that the (010) crystallographic face of the crystals found in the zones of movement within the landslide of this report are also normal to the flat dimension of the crystals.

Morgenstern (1967) suggested that the growth of gypsum in stiff clays weakened the host material due to the volume increase in the transition from sulfide to sulfate. Chandler (1973) observed a distortion of laminar fabric caused by the growth of gypsum crystals. Russell and others (1978), noted a shear-strength anisotropy in weathered Oxford Clay of Great Britain related to chemical weathering, which included the oxidation of sulfides and the growth of gypsum crystals. In that study, correlations indicate the destruction of pyrite caused weakening, whereas gypusm content has no control over shear strength. In Pennsylvania, structural problems are associated with black carbonaceous shales containing sulfide minerals (Dougherty and Barsotti, 1972). After alteration the sulfates are as much as eight times the volume of the sulfide mineral, and it is thought that a 191 to 478 kPa load is necessary to resist uplift forces of crystal growth. Sulfide content as low as 0.1 percent is considered sufficient to warrant corrective measures. Dissolution of particulate gypsum is thought to produce cavities, to cause settlement, and to accelerate seepage flow in foundations of hydraulic structures (James and Lupton, 1978).

Concentrations of gypsum crystals found in the zones of movement suggest the possibility of an osmotic gradient that may attract water into the zone. Gray (1969) described a capillary rise-evaporation cycle that concentrates salts at the top of the capillary zone, creating an osmotic head that draws more moisture. Veder (1972) reported the occurrence of landslides at the weathered-unweathered boundary of soil layers where water accumulates due to a difference in electric potential. Stabilization of several slides was achieved, according to Veder, by short-circuiting the system with iron rods connecting the different layers.

In contrast, a study by Gould (1960) negated the importance of the weathering process as a factor in slope failure in a somewhat similar physical setting. Gould reported iron staining and growths of gypsum crystals in the weathered part of the bituminous, clay-bearing and landslide-prone Modelo Formation in a semiarid region near the Santa Monica Mountains in California. Although the weathered material of the Modelo Formation has a lower sampler penetration resistance and higher water content than the parent material, Gould concluded, on the basis of compositional analysis and strength testing, that the physico-chemical changes accompanying weathering tend to make that weathered soil stronger than the parent material.

The association of gypsum crystals, carbonaceous material, and weak clay zones in the landslide of this study points to the need for further study to examine the effect of composition and the weathering process on slope stability. A comprehensive study comparing the strength and compositional characteristics of weathered slope materials to that of equivalent unweathered material would be of particular interest.

CONCLUSIONS

Seasonal creep occurs in the weathered zone of the failed slope during and shortly after periods of spring thaw and snowmelt.

Displacement profiles are comprised of three elements that define differing zones of behavior within the slide mass; an upper curvilinear element interpreted as surface creep, a middle, near-vertical rigid element of little or no displacement, and a curvilinear element that defines a lower creep zone.

Seasonal creep may have conditioned the slope prior to the initial failure such that lower-than-peak strengths were mobilized.

The initial failure in the spring of 1973 and the sudden renewed failure in mid-May of 1978 were triggered by unusual amounts of precipitation and were centered in the lower zone of creep, defined by inclinometer measurements.

Previous stability analyses based on strength parameters of silty clay (Ebaugh, 1977) probably represent an overestimate of the stability of the slope prior to the initial failure.

Thin, weathered carbonaceous clays with concentrations of small gypsum crystals are weak zones that partly control the location of failure and tend to reduce slope stability.

The orientation and location of the failure surface is largely the result of the combined effect of lithostratigraphic and weathering controls.

High pore pressure detected at one location at the head of the slide probably contributed to the driving forces but may not have been a necessary precondition for the initial failure.

REFERENCES

Bishop, A. W., and Henkel, D. J., 1957, The measurement of soil properties in the triaxial test: London, Edward Arnold Ltd., 190 p.

Booy, E., 1978, Effects of mineralogical variation on stability of soils involved in landslides in northern and central Wyoming, in Symposium on Engineering and Soils Engineering, 16th Annual, Boise, Idaho, 1978, Proceedings: Boise, Idaho Department of Highways, p. 121-135.

Chandler, R. J., 1973, A study of structural discontinuities in stiff clays using a polarising microscope, in International symposium on soil structure, Gothenburg, 1973, Proceedings: Swedish Geotechnical Society, Swedish Society for Clay Research, p. 78-84.

Chleborad, A. F., Nichols, T. C., Jr., and Ebaugh, W. F., 1976, A preliminary inventory, description, and statistical evaluation of landslides in a region of projected urban development, Sheridan, Wyoming: U.S. Geological Survey Open-File Report 76-571, 105 p.

Dougherty, M. T., and Barsotti, N. J., 1972, Structural damage and potentially expansive sulphide minerals: Association of Engineering Geologists Bulletin, v. 9, no. 2, p. 105-125.

Eardley, A. J., and Stringham, B. F., 1952, Selenite crystals in the clays of Great Salt Lake [Utah]: Journal of Sedimentary Petrology, v. 22, no. 4, p. 234-238.

Ebaugh, W. F., 1977, Landslide-factor mapping and slope-stability analysis of the Big Horn quadrangle, Sheridan County, Wyoming: Boulder, Colorado University Ph. D. thesis, 194 p.

Ebaugh, W. F., Olsen, H. W., and Bennetti, J. B., 1977, A new technique used for inclinometer casing installation: Association of Engineering Geologists Bulletin, v. 14, no. 4, p. 277-282.

Fukuoka, M., 1953, Landslide in Japan, in International Conference on Soil Mechanics and Foundation Engineering, 3d, 1953, Proceedings: v. 2, p. 234.

Gould, J. P., 1960, A study of shear failure in certain Tertiary marine sediments, in Manual of shear strength of cohesive soils: American Society of Civil Engineers, Boulder, Colorado, p. 615-641.

Gray, D. H., 1969, Prevention of moisture rise in capillary systems by electrical short circuiting: Nature, v. 223, no. 5204, p. 371-374.

Grim, R. E., 1962, Applied clay mineralogy: New York, McGraw-Hill, 422 p.

James, A. N., and Lupton, A. R. R., 1978, Gypsum and anhydrite in foundations of hydraulic structures: Geotechnique, v. 29, no. 3, p. 249-272.

Kim, M. M., and Ko, H., 1977, Multi-stage triaxial testing: U.S. Bureau of Mines Report of Investigation, 87 p.

Kirkby, M. J., 1967, Measurement and theory of soil creep: Journal of Geology, v. 75, no. 4, p. 359-378.

Krauskopf, K. B., 1967, Introduction to geochemistry: New York, McGraw-Hill, p. 275.

Lambe, T. W., and Whitman, R. V., 1969, Soil mechanics: New York, John Wiley and Sons, 553 p.

Mapel, W. J., 1959, Geology and coal resources of the Buffalo-Lake De Smet area, Johnson and Sheridan Counties, Wyoming: U.S. Geological Survey Bulletin 1078, 148 p. [1961].

McKenna, M. C., and Love, J. D., 1972, High-level strata containing early Miocene mammals on the Bighorn Mountains, Wyoming: American Museum Novitates, no. 2490, 30 p.

Miller, C. H., 1979, Seismic, magnetic, and geotechnical properties of a landslide and clinker deposits, Powder River Basin, Wyoming and Montana: U.S. Geological Survey Open-File Report 79-952, 42 p.

Morgenstern, N. R., 1967, Shear strength of stiff clay, in Shear Strength Properties of Natural Soils and Rocks: Norwegian Geotechnical Institute, Geotechnical Conference, Oslo, 1967, Proceedings, v. 2, p. 59-69.

National Climatic Center, 1974, Local climatological data--Annual summary with comparative data, Sheridan, Wyoming: Asheville, N.C., U.S. Department of Commerce, National Climatic Center, 6 p.

_____1977, Local climatological data--Monthly summary (March, April), Sheridan, Wyoming: Asheville, N.C., U.S. Department of Commerce, National Climatic Center, 1 p.

_____1978, Local climatological data--Monthly summary (March, April), Sheridan, Wyoming: Asheville, N.C., U.S. Department of Commerce, National Climatic Center, 1 p.

Obernyer, S. P., 1978, Basin-margin depositional environments of the Wasatch Formation in the Buffalo-Lake De Smet area, Johnson County, Wyoming, in Symposium on the Geology of Rocky Mountain Coal, 2d, Colorado Proceedings: Colorado Geological Survey Series no. 4, p. 49-65.

Russell, D. J., Denness, B., and McCann, D. M., 1978, Shear-strength anisotropy variations in weathered Oxford Clay: Engineering Geology, v. 12, no. 4, p. 337-344.

Sharpe, C. F. S., 1938, Landslides and related phenomena: New York, Copper Square Publications, p. 21.

Taff, J. A., 1909, The Sheridan coal field, Wyoming, in Coal fields of Wyoming: U.S. Geological Survey Bulletin 341-B, p. 123-150.

Tchourinov, M. P., 1945, Modifications by weathering in the composition, structure, and properties of the lower Cretaceous clay: Doklady Novaia Seriia, v. 49, no. 5, p. 364-368.

Ter-Stepanian, G., 1965, In situ determination of the rheological characteristics of soils on slope, in International Conference on Soil Mechanics and Foundation Engineering, 6th, Proceedings: p. 575-577.

Terzaghi, Karl, 1950, Mechanism of landslides, in Application of geology to engineering practice: Geological Society of America Berkey Volume, p. 83-123.

Veder, C., 1972, Phenomena of the contact of soil mechanics: International Symposium on Landslide Control, Kyoto and Tokyo, Japan Society of Landslide, 1972, p. 143-162. (In English and Japanese.)

APPENDIX

The biaxial miniprobe used in the study is 45.7 cm in length, 2.5 cm in diameter, and has a 30.5 cm wheelbase. The sensors consist of two fluid-damped metal flexure accelerometers mounted in a housing at the end of the probe. The sensitive axes are mounted 90° apart such that one axis (A axis) measures the component of tilt towards or away from the probe's spring-loaded wheels. The other sensor (B axis) measures tilt 90° to the A axis. Individual readings are considered accurate to ±0.005 cm. Calibration checks were made periodically using a modified transit. The transit was adapted by removing the eyepiece and lens of the scope and using the scope as a mount for the probe (wheels removed). A brass collar machined to within 0.02 mm I.D. (inside diameter) of the probes diameter was fitted to the upper end of the scope. Set screws in the brass collar and at the other end of the scope allowed positioning and securing of the probe. To check the calibration, the probes position was set to vertical by adjusting the set screws until zero or near zero output was obtained on the readout. Incremental angular changes were made over the total range of sensitivity (±25°) using the transits vernier to measure angle changes. A typical set of data is presented in table 2. Field measurements were made by lowering the probe to the bottom of the casing with the springloaded wheels (A axis) in a casing keyway oriented downslope in the general direction of anticipated movement and recording at 0.305 m intervals as the probe was raised. The downslope orientation of one axis increased the possibility of detecting small movements near the limit of detectability. The probe was then rotated 180°, and the process was repeated. This procedure eliminates an offset term that results from system output when no deviation from the zero reference orientation (true vertical) is present. Incremental displacement changes were obtained by algebraically

averaging complementary readings and then subtracting an initial set of readings used as datum. Cumulative sums were calculated from the bottom of the hole up, and relative change in displacement of the borehole was determined by subtracting initial cumulative sums and plotting the differences.

Table 2.--Typical calibration check data set for one axis of the biaxial miniprobe digital inclinometer

Probe orientation (α) (degrees from vertical)	A-axis calibration check		
	Instrument output (X) (inches deflection)	Indicated orientation (θ) (degrees $= \sin^{-}(\frac{X}{12"})$	Indicated error (inches deflection $= \sin\alpha - \sin\theta$)
0	+0.004	+ 0.02	<0.001
- 5	-1.034	- 4.9	.001
-10	-2.071	- 9.9	.002
-15	-3.087	-14.9	.002
-20	-4.077	-19.9	.003
-25	-5.039	-24.8	.003
0	.001	- .01	< .001
+ 5	+1.036	+ 4.9	.001
+10	+2.069	+ 9.9	.002
+15	+3.083	+14.9	.002
+20	+4.075	+19.9	.002
+25	+5.036	+24.8	.003

The electric piezometers that were used are approximately 15 cm long, 2.5 cm in diameter, and have a pressure range from 0 to 250 psi. An accuracy of 0.25 percent on full-scale is indicated by the manufacturer. The instruments were tested prior to field installation by subjecting them to varying hydrostatic heads in a 3 m drill hole. An electric control unit with a readout in feet of water was used to monitor the piezometers. Plastic tubing (1.8 cm I.D.) was used for the well-point piezometers. The tubes are open ended and, like the electric piezometers, were installed in the drill holes using sand filters and bentonite seals above and below the zone of interest. Figure 27 dipicts the two types of piezometer installations.

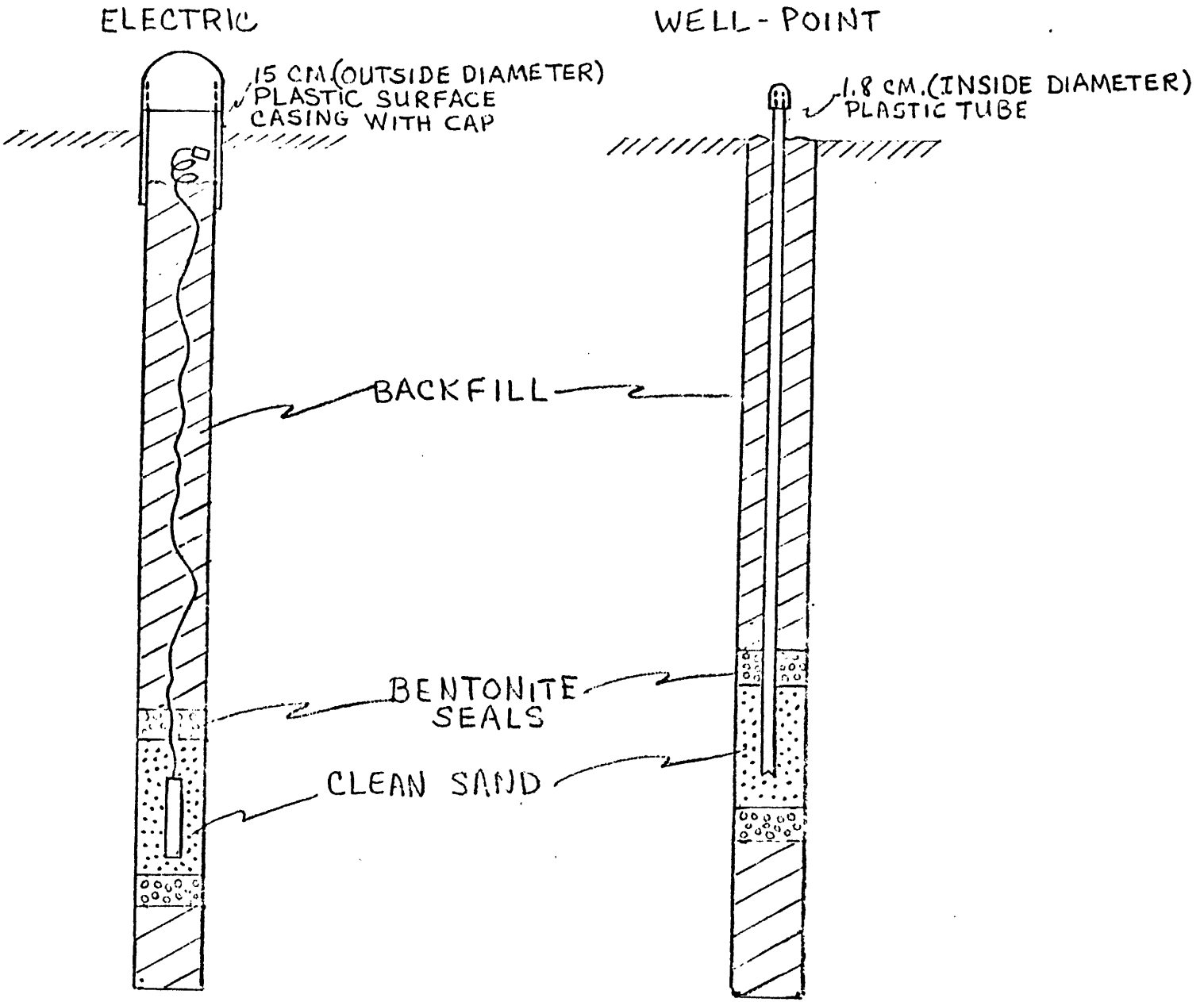

FIGURE 27. ELECTRIC AND WELL-POINT PIEZOMETER INSTALLATIONS.
(DRAWING NOT TO SCALE.)